

Review

A review of in-situ monitoring and process control system in metal-based laser additive manufacturing



Yuhua Cai^a, Jun Xiong^{a,b,*}, Hui Chen^a, Guangjun Zhang^b

^a Key Laboratory of Advanced Technologies of Materials, Ministry of Education, School of Materials Science and Engineering, Southwest Jiaotong University, Chengdu 610031, China

^b State Key Laboratory of Advanced Welding and Joining, Harbin Institute of Technology, Harbin 150001, China

ARTICLE INFO

Keywords:

Laser additive manufacturing
Metal
In-situ monitoring
Process control
Review

ABSTRACT

Metal-based laser additive manufacturing (MLAM) is receiving significant attention in industrial fields due to its capacity to manufacture complex and high-performance metal components directly from three-dimensional models. However, as-built components are still subjected to various issues, such as dimension accuracy, surface quality, and internal defects, seriously hindering the development of MLAM. To overcome these issues, process monitoring and control in MLAM should be emphasized to achieve high-quality parts. Taking the critical segments of a closed-loop control system in MLAM as the research route, this paper aims to develop an in-depth survey of in-situ process sensing and control strategies in MLAM. Various signal monitoring methods are described, principles of induced defects and corresponding scientific control strategies are introduced, and closed-loop control strategies in MLAM are summarized. The current development status and limitations of sensing methods and closed-loop control frameworks are discussed. The paper concludes by advising the future research directions for in-situ monitoring, process control, and performance of machine learning models in MLAM. This review provides a valuable reference and a blueprint for developing advanced intelligent control of MLAM in industrial applications.

1. Introduction

With the development of computer-aided design and manufacturing technologies, additive manufacturing (AM) is receiving significant attention since it can slice complex three-dimensional (3D) structures into two-dimensional layers and further melt and stack materials layer by layer to directly drive the production of parts [1,2]. This technology can fabricate components with complex internal structures and low buy-to-fly ratios. It is regarded as a revolutionary technique in industrial fields once proposed [3,4] and has been widely applied in medical, aviation, military, and other cutting-edge industries. Compared with traditional polymer-based AM, metal-based AM using materials with

high melting points has broader application prospects, but its technical complexity increases exponentially. At present, heat sources in metal-based AM can be a laser beam, an electron beam, and an arc [5]. Among them, electron beam AM has strict requirements for a vacuum chamber, and the chamber volume limits the size of fabricated parts. Wire and arc additive manufacturing (WAAM), using an arc as the heat source and wire as filler materials, has unique advantages for building large-scale components due to high production efficiency. However, the dimensional accuracy of parts deposited in WAAM is unsatisfactory. Considering as-built components' manufacturing sizes and accuracy, the laser is currently regarded as the ideal heat source in metal-based AM [6, 7].

Abbreviation: AM, additive manufacturing; 3D, three-dimensional; MAM, metal-based additive manufacturing; MLAM, metal-based laser additive manufacturing; WAAM, wire and arc additive manufacturing; PBF, powder bed fusion; LPBF, laser powder bed fusion; LDLED, laser direct energy deposition; P-LDED, powder-based laser direct energy deposition; W-LDED, wire-based laser direct energy deposition; ML, machine learning; AE, acoustic emission; IR, infrared; NDT, non-destructive testing; NIR, near infrared; CNN, convolutional neural network; CCD, charge-coupled device; CMOS, complementary metal-oxide-semiconductor; OES, optical emission spectroscopy; ICI, inline coherent imaging; APC, automatic process control; FEM, finite element model; PI, proportional-integral; PID, proportional integral derivative; ANFIS, adaptive network fuzzy inference system.

* Correspondence to: Key Laboratory of Advanced Technologies of Materials, Ministry of Education, School of Materials Science and Engineering, Southwest Jiaotong University, 111, Section 1 North Second Ring Road, Chengdu 610031, China.

E-mail address: xiongjun@home.swjtu.edu.cn (J. Xiong).

<https://doi.org/10.1016/j.jmansy.2023.07.018>

Received 29 April 2023; Received in revised form 17 July 2023; Accepted 29 July 2023

Available online 8 August 2023

0278-6125/© 2023 The Society of Manufacturing Engineers. Published by Elsevier Ltd. All rights reserved.

Currently reported metal-based laser additive manufacturing (MLAM) technologies mainly include **laser powder bed fusion** (LPBF) and **laser directed energy deposition** (LDED) (Fig. 1). LDED is divided into powder LDED (P-LDED) and wire LDED (W-LDED) based on the feedstock form difference. The LPBF technique uses a low-power laser (hundreds of watts) to melt the powder selectively based on the slice geometry. The average layer thickness is about 20–100 μm due to the small molten pool size [8]. Hence, the dimensional accuracy of parts in LPBF is well controlled. However, production efficiency and size limitation are the main shortcomings of LPBF. The material melting rate of LPBF ranges from 0.01 to 0.2 kg/h [4], and the component sizes are subject to the laser scanning range [7]. LDED has a higher manufacturing efficiency and can provide a larger process parameter window than LPBF. Moreover, parts fabricated in LDED exhibit excellent structure density and metallurgical bonding. LDED is also widely used for surface repair and coating preparation [9]. When it is used to build large structures, many researchers recommend using wires to replace powders as feedstocks to decrease manufacturing costs [10]. However, defects, such as molten pool collapse, low dimensional accuracy, and coarse grains, occur more easily in LDED than in LPBF due to the increasing heat input [11,12].

Since the birth of MLAM, large-scale applications of this technique have been plagued by quality assurance, dimensional accuracy, and degree of automation [13,14] because the process parameters in MLAM are quite sophisticated. The physical phenomena induced by the interaction of laser beam and metal material are quite complex, posing serious disturbances in MLAM. Imposing process control is a highly effective approach to produce repeatable, reliable, and quality-ensured parts in MLAM. In general, developing a closed-loop control system involves monitoring physical signals, modeling the relationship between process parameters and physical signals, and designing control algorithms to realize the accurate regulation of process parameters. From sensing devices to data processing algorithms and process control theories, the progress of each step presents a considerable challenge to researchers [15–17].

Marked effects have been achieved on the quality optimization of components in MLAM by integrating an intelligent closed-loop control module, including process sensor signals, regulated process parameters, and final parts' characterizations, such as dimensional accuracy, internal defects, and mechanical properties. Clarifying the qualitative and quantitative relationships between sensing methods and physical signals is essential, especially the fusion optimization strategy of multiple signals and control objects. Integrating an intelligent system with learning and self-renewal capabilities into process control is a research hotspot for achieving high-precision decision-making and rapid optimization.

In recent decades, numerous research efforts have been conducted to create a complete data stream, monitoring, modeling, and control ecosystem in MLAM. However, these studies are sparse and need more systematic summarization and unique insights into future research directions in a single source. Therefore, this article reviews the current research status of in-situ monitoring and process control technologies in

MLAM and provides inspirations and strategies for creating a closed-loop control ecosystem based on data-driven in the future.

Recently, a comprehensive review of additive manufacturing was published by Xia et al. [15]. This review focused on the monitoring and control system of WAAM and the welding process instead of laser AM. Another review of MAM was published by Lin et al. [18]. It mainly focused on the monitoring system of MAM, including sensing data acquisition, image and signal processing, and intelligent algorithms for quality monitoring and classification. This paper aims to clarify defect control methods in three types of MLAM, i.e., LPBF, P-LDED, and W-LDED, highlighting the monitoring technologies and control strategies based on closed-loop control frameworks. Specifically, this paper describes sensing techniques' development levels and limitations under specific MLAM processes. Defect types that are prone to occur during the MLAM process are summarized, and corresponding suppression measures are analyzed. Further, the development history of process closed-loop control is retraced, and an ML-based intelligent control framework is proposed. The research status of closed-loop control in MLAM is reviewed. Finally, future development directions of in-situ monitoring, process control, and machine learning (ML) model performance are advised. Fig. 2 displays the review roadmap of this article.

This article is organized as follows. Section 2 briefly overviews physical signal types in MLAM and related monitoring technologies. Section 3 concludes the influential factors of geometries and internal defects for components in MLAM. Section 4 introduces frameworks of the traditional closed-loop control and the emerging ML-based control. Further, this section reviews the research literature on process control in LPBF, P-LDED, and W-LDED. Section 5 concludes this article. Section 6 points out the future research directions of process monitoring and control in MLAM. This review systematically introduces the latest developments, discoveries, and technologies for quality control in MLAM, providing important reference materials for scholars currently focusing on this field. This review can also guide the development of automation systems for other AM technologies.

2. Signal sensing

Signal sensing, regarded as a fundamental part of a closed-loop control system, has been applied in almost all industrial fields. The scientific configuration between physical signals and monitoring methods has a profound significance for process control in MLAM. In-situ signals generated in the MLAM process are divided into visual, thermal, spectral, and acoustic emission (AE) signals. Table 1 shows the sensing signals and monitoring objects in MLAM.

2.1. Principle of signal monitoring in MLAM

The interaction between laser energy and metal materials is intricate. Components fabricated in MLAM undergo a rapidly changing thermo-physical metallurgical process. The physical processes in MLAM include materials melting and solidification, plasma eruption, Marangoni

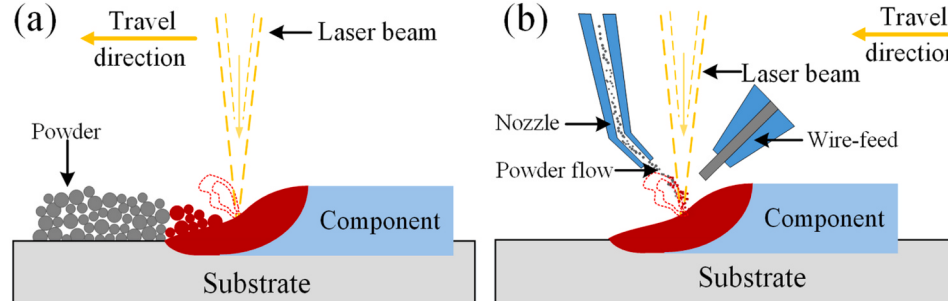


Fig. 1. Schematic diagram of two types of laser additive manufacturing. (a) Laser powder bed fusion. (b) Laser direct energy deposition.

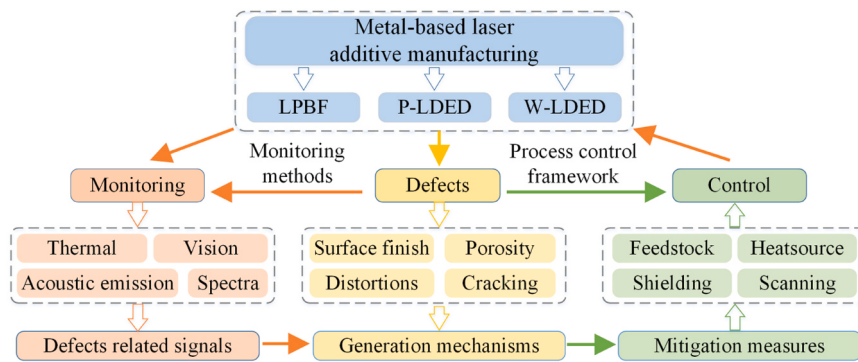


Fig. 2. Roadmap of this review.

Table 1
Sensing signals and monitoring objects in MLAM.

Signal	Monitoring object	Sensor equipment	Literature		
			LPBF	P-LDED	W-LDED
Thermal signals	Molten pool temperature & Molten pool geometry characteristics & Plume & Defects	Pyrometer & Photodiode & IR camera & NIR camera & hyperspectral line camera & Optical spectrometer	[20,27,28,31,32,34–36,38,62–64,138,140,142,150]	[25,26,29,30,33,37,151,154,163–170]	[172–174]
Vision signals	Molten pool dimension & Molten pool geometry characteristics & Spatter & Plume & Deposited layer geometry characteristics & Defects	CCD & CMOS & ICI & Line camera & 3D camera system	[20,22,41,43,48,49,52–55,57–59,99,101,141,147]	[24,44–47,50,51,56,60,152,153,156,157,159–162]	[171,175,176,180]
Acoustic signals	Defects	Structural load acoustic emission sensor & Microphone & Fiber Bragg Grating sensor	[61–64,69–75,77,79]	[56,65,67,68,76]	
Spectral signals	Plasma characteristics & Phase transformation & Defects & Spatter	Spectrometer	[83,86]	[81,82,85]	[84]

convection, heat conduction, and radiations [19]. Rapidly changing temperature fields, acoustic waves, visible lights, ultraviolet lights, and infrared (IR) radiations are generated during these physical processes (Fig. 3) [14]. The abnormality of physical signals is directly related to defects generated in MLAM. Rich data related to the quality status of final parts can be obtained by signal monitoring, providing the possibility of real-time identification and online optimization for forming quality [20,21]. These collected data must be treated to extract the feature quantities for machine cognition. Then, mathematical modeling between feature quantities and regulated parameters should be performed [22,23]. This section mainly discusses the main sensing methods that support online monitoring in MLAM.

2.2. Thermal signals

Thermal evolution behavior of materials melting and solidification can be used to clarify the forming mechanisms of internal defects and geometric distortions of components in MLAM [24,25]. Variations in microstructures and forming dimensions of as-built parts, induced by the local thermal difference over time during material processing, lead to inhomogeneous mechanical properties. Compared with other non-destructive testing (NDT) techniques, thermal sensing methods allow more extensive observation ranges and higher installation flexibility [26–28]. Marshall et al. [29] used a pyrometer to detect the molten pool temperature and an IR camera to monitor the dynamic evolution of bulk part temperature. The large-area and high-precision temperature distribution fields in P-LDED were obtained. They further studied the relationship between the thermal behaviors and

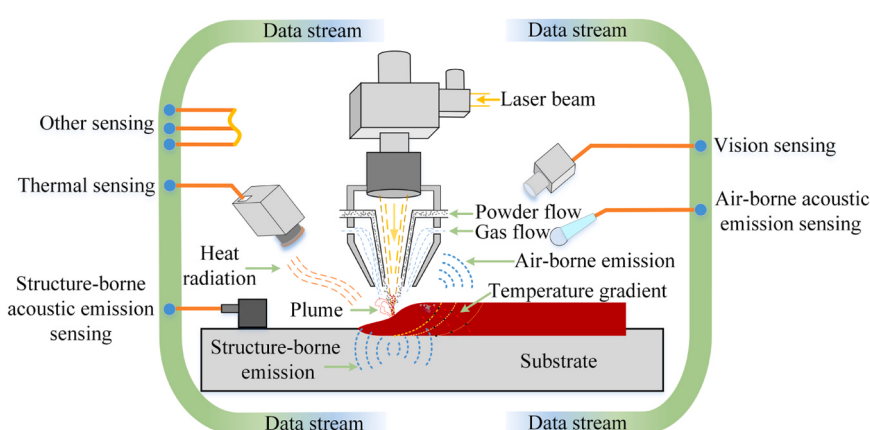


Fig. 3. Schematic diagram of the generation and propagation of physical signals in MLAM.

microstructure of deposited layers [30].

Thermography systems have been widely applied to characterize the molten pool size and diagnose the process stability [31]. Zheng et al. [32] utilized a thermal camera coaxial with the laser beam to monitor the molten pool temperature in LPBF (Fig. 4). The real-time molten pool width was measured by extracting the predefined threshold profile of temperature gradient. Thermography sensing is a high-efficiency method for detecting surface or internal defects of parts in MLAM [33]. Dimer et al. [34] constructed a multi-sensor monitoring system including a near-infrared (NIR) wavelength camera, a visible wavelength camera, and a photodiode to monitor porosities in fabricated parts by analyzing the characteristics of laser absorption rate and the temperature field evolution in LPBF. Mitchell et al. [35] used a two-color pyrometer to monitor the molten pool's instantaneous anomalies in LPBF. ML algorithms were used to handle the collected data. They performed fusion analysis for the macro-computed tomography data to recognize the internal pores of components, showing that the intelligent method can extract the deep features of complex data [36]. The molten pool's radiation spectrum can be used to detect the molten pool temperatures based on the relationship between spectral radiance and measured objects [37]. Devesse et al. [38] used a hyperspectral line camera to capture the spectra of massive closely spaced points on the molten pool surface and achieved the temperature measurement with a spatial resolution of $12 \mu\text{m}/\text{pixel}$ via a nonlinear least-square algorithm, fulfilling the requirement of high-precision temperature measurement in MLAM.

2.3. Vision signals

Vision sensing is a powerful method for extracting local structure features or layer shapes of components in MLAM, such as height, width,

and distortion [39,40]. Furthermore, the recognition of internal defects is frequently studied based on visual information. With the development of ML methods, such as support vector machines and convolutional neural networks (CNN), internal features of components can be extracted from captured images with high efficiency [41,42]. The frequently used visual sensing system is a charge-coupled device (CCD) or a complementary metal-oxide-semiconductor (CMOS) camera with suitable waveband filters.

Visual sensing accuracy is highly related to camera resolution. Visual sensing plays an irreplaceable role in dimension feedback in MLAM. Many studies directly extract the molten pool size based on acquired visual information and image processing algorithms [43,44]. Fig. 5 exhibits the CMOS camera setup of process monitoring in LPBF. Subsequently, a multi-vision sensing framework is proposed for the collaborative analysis of multi-dimensional visual information [45].

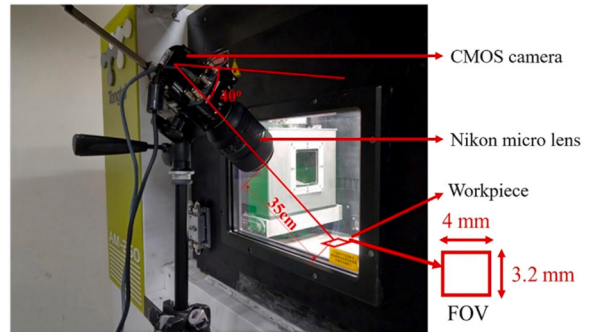


Fig. 5. CMOS camera setup of process monitoring in LPBF [44].

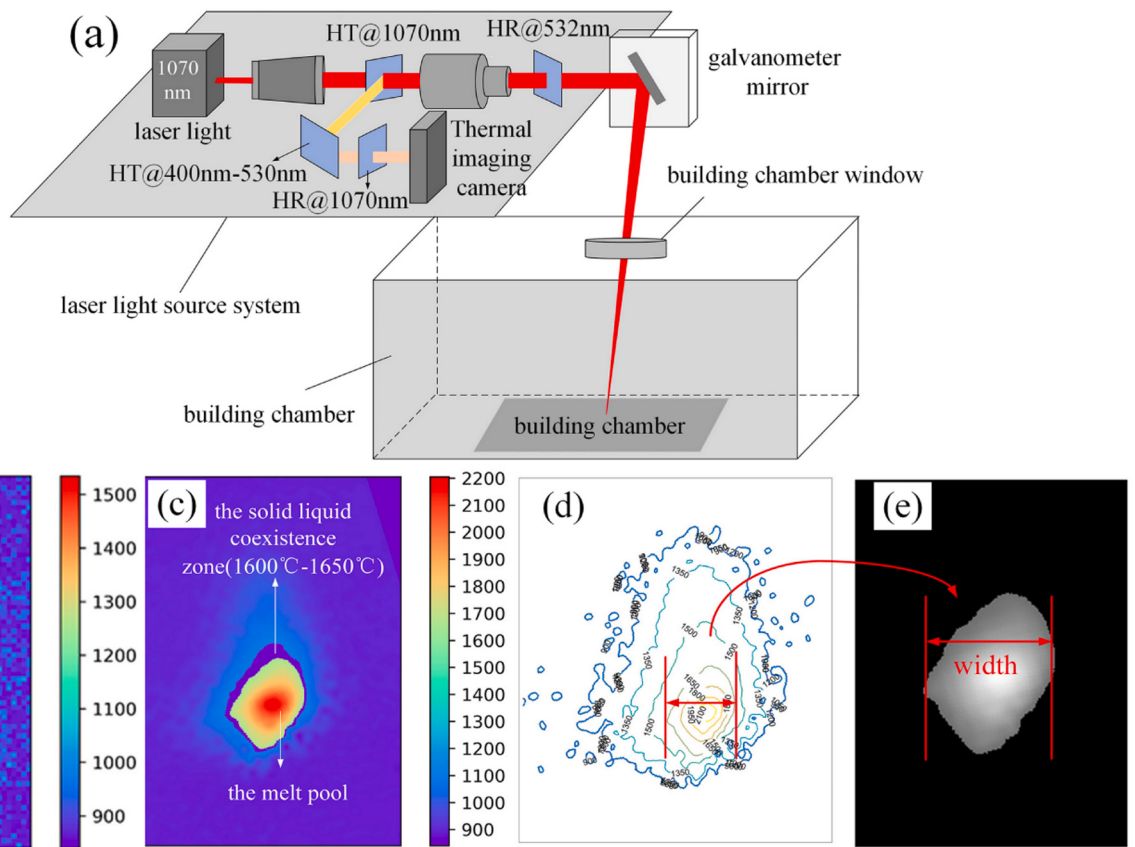


Fig. 4. (a) Schematic diagram of a thermal sensing device. (b) Original thermal stream image. (c) Correcting image. (d) Isotherm diagram. (e) Grayscale of the extracted melt pool [32].

Mehrdad et al. [46] designed a trinocular optical detector consisting of three CCD cameras and developed image processing algorithms with a recurrent neural network to handle the composite image information, achieving the real-time detection of deposition height in P-LDED. Perani et al. [47] established a monitoring system of the molten pool based on a laser coaxial CMOS camera, and the molten pool image and process parameter data were used as the inputs of a combined network to achieve layer geometry prediction in P-LDED. Furthermore, visual data analysis is a feasible method for monitoring and diagnosing the process state [48,49]. Naiel et al. [50] developed a fusion algorithm for image processing to detect the laser-material interaction region in P-LDED based on a high dynamic range camera. The constructed identification system can identify different action modes, including under-melting, conduction, and keyhole melting, with an accuracy of over 90%. Sun et al. [51] used a coaxial visual system to monitor the molten pool evolution in P-LDED and proposed a prediction method of crystal growth behavior based on the molten pool contour. Kim et al. [52] trained a CNN model with molten pool images in LPBF and established an estimation system of beam scan direction based on the trained model.

Internal defects in components built by MLAM are invisible. Currently, internal defect detection highly depends on post-processing methods. However, many studies are devoted to developing in-situ methods for rapid positioning and quantification of defects based on visual sensing [53,54]. Felix et al. [55] combined a recoater-based line camera and a 3D measurement system to construct a high-resolution optical monitoring system for recognizing layer deviation defects in LPBF. They extracted the brightness and periodicity features of the images and achieved a resolution of 5.97 $\mu\text{m}/\text{pixel}$ based on the relationship between the extracted features and the forming quality. Fig. 6 illustrates the images processed during the experiment. ML methods and intelligent algorithms have presented a tremendous potential for extracting image information's size and timescale characteristics [56, 57]. Scime et al. [58] used a high-speed camera to monitor the porosity and balling flaw in LPBF. They established a correlation between the molten pool morphology and in-situ defect characteristics. Wang et al. [59] established a semantic segmentation model to detect the stratified

defects in LPBF with layer image data. Then, unsupervised ML techniques were utilized to classify the molten pool to identify defects with high efficiency. Ahmad et al. [60] captured a sequence of molten pool images in LDED by a CCD camera and used an intelligent Particle Swarm Optimization algorithm to predict the molten pool geometry. Furthermore, the process parameters and geometric features were modeled, and a Self-organizing Pareto-based Evolutionary algorithm was used to find the optimal process parameters.

2.4. Acoustic emission signals

Vision and thermal signals possess irreplaceable advantages in monitoring shallow and external physical characteristics. However, these signals cannot reflect the internal state of deposited components. The transient elastic waves are excited from the molten pool during the complex thermomechanical interaction between the laser beam and metal materials [61]. These waves carry much information associated with internal characteristics, such as pores and cracks [62]. As shown in Fig. 7, the AE signals exhibit significant differences due to various porosity levels [63]. As time-dependent one-dimensional data, AE signals can be processed rapidly, and the sensing and analyzing system's costs are low [64–66]. Therefore, developing AE sensing technologies is valuable for defect detection in MLAM. The AE signals for sensing mainly include structural-borne AE, air-borne AE, and ultrasonic signals.

A contact-type piezoelectric sensor commonly monitors structural-borne AE signals. Gaja et al. [67] combined the principal component analysis and the K-means clustering method to construct a defect recognition system via the structural-borne AE signals. They used AE signals' time domain and frequency domain to characterize the sources of cracks and pores in P-LDED. Li et al. [68] utilized a CNN model to extract the feature vectors of the AE signals sampled in P-LDED. These feature vectors can identify the cladding quality diagnosis and crack defects. Fig. 8 exhibits the framework of the cladding state recognition and crack diagnosis model. Ito et al. [69] integrated an online monitoring system constructed by two AE sensors into the LPBF process. The system can determine the micro-cracks and pores' occurrence time and

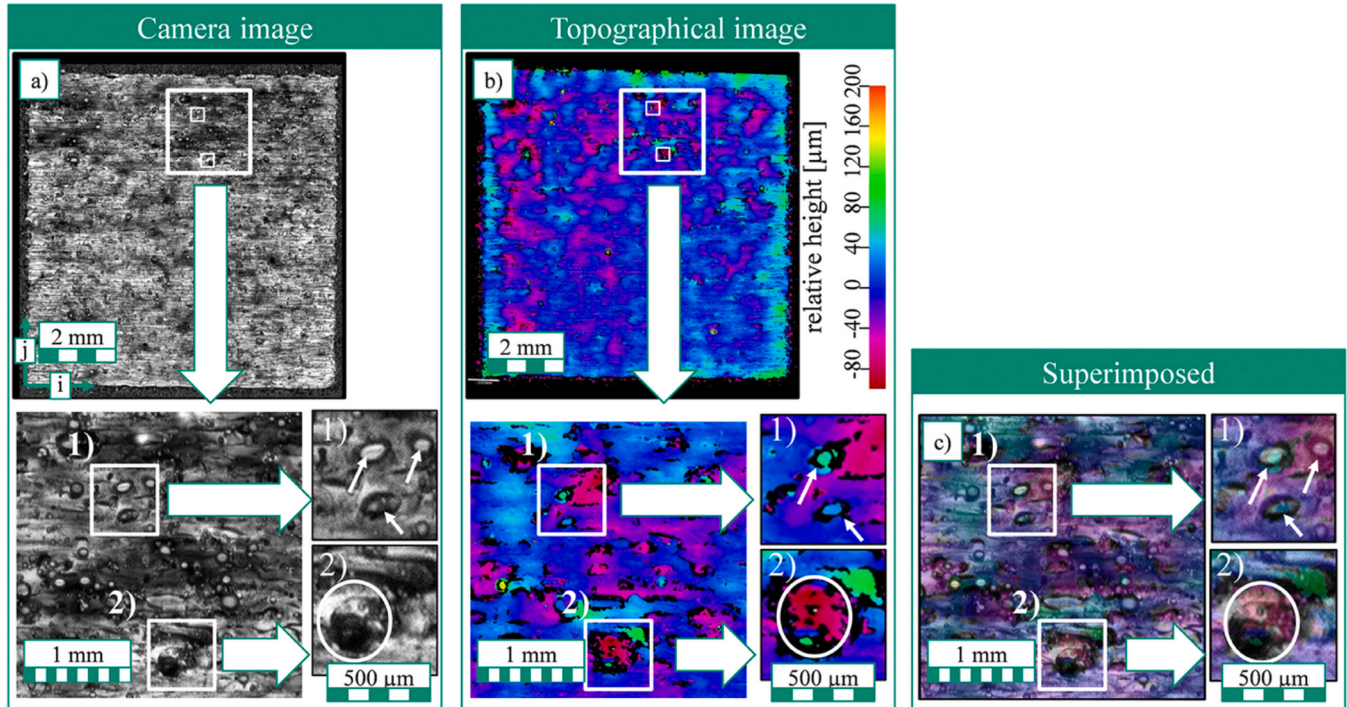


Fig. 6. Samples' top layer images obtained by different monitoring equipment: (a) In-situ camera system. (b) Ex-situ using the Alicona Infinite Focus. (c) Superposing both images. (1) Spatters in both images. (2) A significant irregularity [55].

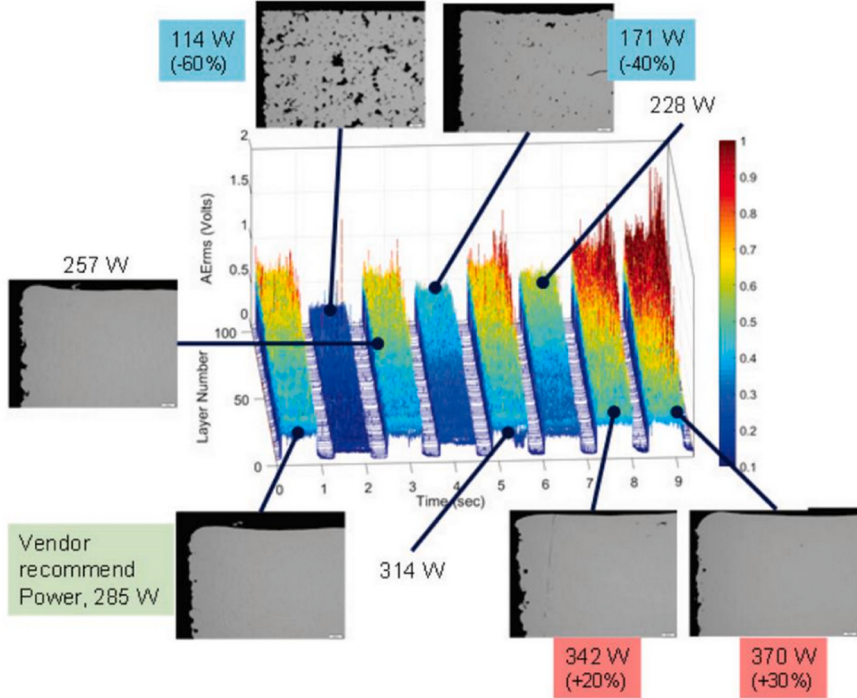


Fig. 7. Root mean squared filtered AE signals associated with porosity [63].

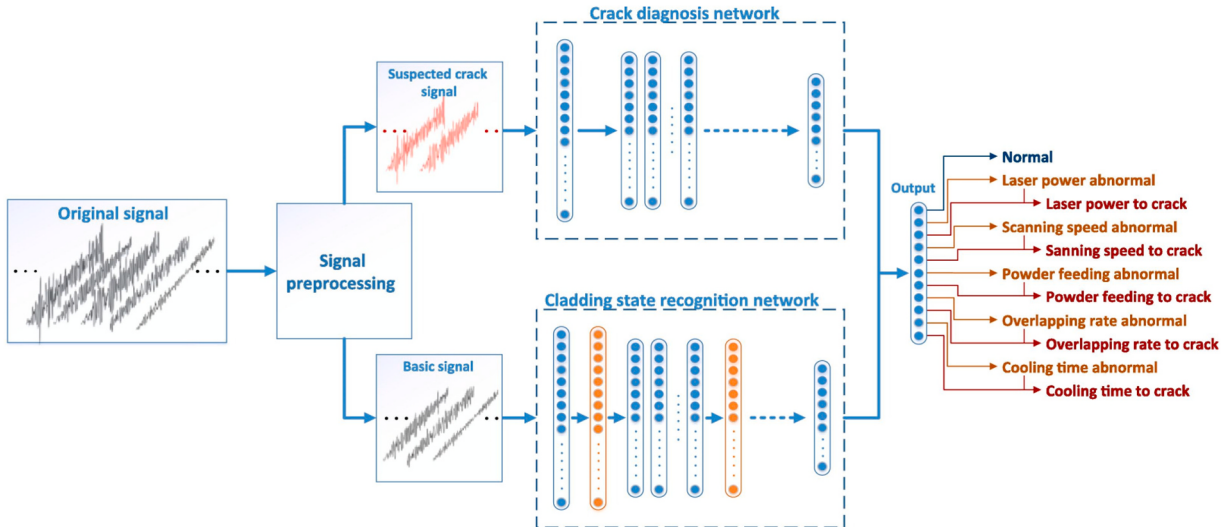


Fig. 8. Framework of the cladding state recognition and crack diagnosis model [68].

location based on the AE signals' time domain and amplitude difference. The system's spatial positioning error was within 2–3 mm. Kononenko et al. [70] created an in-situ monitoring system to monitor the crack defects in LPBF based on AE sensing and an ML model. They found that using the spectral components of AE signals as the ML model's input can achieve the best prediction accuracy.

Air-borne AE sensing can minimize structural noises and realize flexible installation. Ye et al. [71] used a microphone to collect the AE signals in LPBF and established the mapping between the AE signals and the process parameters. They used a deep belief network for defect recognition based on the AE signals and found that the intelligent recognition method had higher accuracy and efficiency than traditional algorithms [72]. Pandiyan et al. [73] studied AE characteristics under various laser regimes in LPBF, including balling, lake-of-fusion, no pores, and keyhole, indicating that the laser energy density was the

dominant factor affecting the melting mode and the AE characteristics.

Ultrasonic signals have been widely applied in NDT due to the characteristics of short wavelength and excellent directionality. Since the ultrasonic wave is difficult to be generated spontaneously, auxiliary equipment is required in MLAM [74]. Allam et al. [75] integrated an ultrasonic sensing device into the LPBF system and used an incident probe with a frequency of 10 MHz to generate longitudinal waves. The dynamic behavior of the backwall echo depicted the formation of pores in LPBF. Laser ultrasound, introduced by a reversible thermoelastic deformation of materials, is a promising technology for defect detection in MLAM [76,77]. Dai et al. [78] integrated a laser ultrasonic device into the LPBF system and realized the in-situ identification of sub-millimeter crack defects with a depth of 0.5 mm. Moreover, the crack defects' positions and dimensions were determined by the Lamb waves' behavior. Lv et al. [79] used a Doppler vibrometer to collect the ultrasonic waves

in LPBF with a high signal-to-noise ratio. The ultrasonic waves were induced by a pulsed laser. A Rayleigh wave with a circular scanning strategy was first proposed to achieve the quantification and localization of defects.

2.5. Spectral signals

Metal elements in the excited state will release unique characteristic spectral lines. Therefore, optical emission spectroscopy (OES) is regarded as an excellent tool for compositional analysis in MLAM [80,81]. OES exhibits high analysis speed and sensitivity and has been widely applied for monitoring process conditions and understanding physical mechanisms in MLAM.

In general, the intensity ratio of characteristic spectral lines is proportional to elemental concentration [82]. Lough et al. [83] used OES to collect the spectra information of emitted lights in LPBF, analyzed the chemistry and relative intensities of excited species, and systematically studied the correlation between the spectral characteristics and the process parameters. Fig. 9 shows the specific conclusions. Liu et al. [84] studied the relationship between the deposition stability and spectral characteristics in resistance hot-wire LDED, finding that productivity increased markedly when the hot-wire voltage was applied. However, arc plasma and spatters were generated, and OES features changed markedly when the hot-wire voltage exceeded 12 V. As an in-situ technique, OES has shown a significant potential to characterize internal defects in MLAM [85]. As described by Montazeri et al. [86], the spectra signals in LPBF were Fourier transformed, and tomography detection was used to quantify pores. Fourier transform coefficients were used as input to train an ML model to realize the pores prediction, and the model's prediction accuracy reached 90%.

2.6. Section summary

The references above show that significant progress on sensing devices and strategies in MLAM has been gained. Thermal sensing can

monitor local and bulk thermal behaviors of as-built components. The geometric features of deposited layers can be extracted by treating the temperature distribution of components. Visual sensing is the most common technique to extract morphological features, such as surface defects and dimension deviations. Although sensing methods developed for monitoring thermal and visual signals possess high accuracy and wide measurement ranges, they may cause lag effects due to relatively long processing time. AE and spectra signals are more suitable for monitoring the internal states of deposited parts. However, the feature extraction of AE or spectra signals depends on complex data processing algorithms. Fig. 10 summarizes the characteristics of different signal-sensing systems applied in MLAM.

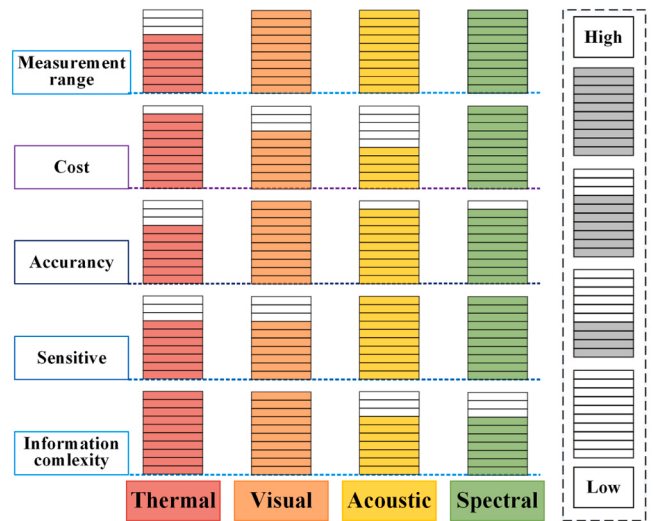


Fig. 10. Characteristics of different signal sensing systems.

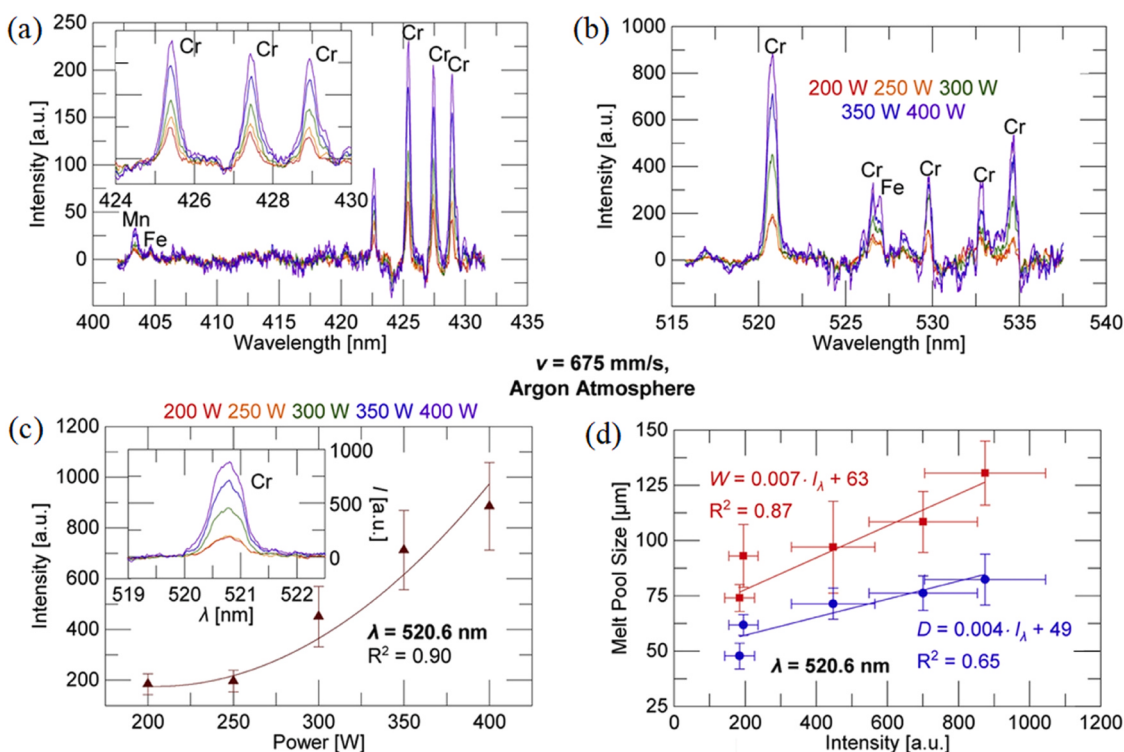


Fig. 9. Average OES for wavelength ranges plotted from: (a) 400–435 nm and (b) 515–540 nm. (c) Average intensity of chromium emission around a wavelength of 520.6 nm. (d) Average melt pool size of single layers plotted versus average intensity of chromium emission for corresponding layers [83].

3. Principle of forming accuracy and quality

The thermophysical effect and non-equilibrium metallurgy of metal materials in MLAM are complicated [87,88]. Components fabricated by MLAM will experience violent laser-material interactions, the molten pool's rapid solidification under strong constraints, grain growth under extreme temperature gradients, unstable manufacturing atmospheres, and high-cycle thermal stress. Abnormalities occurring in any aspect during manufacturing will induce various quality issues and even unusable parts. The quality issues encountered in MLAM vary due to different patterns in laser-matter interactions [89,90]. These issues can be divided into two categories, i.e., dimensional accuracy and internal defects. This section discusses the generation mechanism and mitigation methods for defects, providing a basis for quality control in MLAM. Fig. 11 summarizes the defect types and their corresponding mitigation measures in MLAM.

3.1. Dimensional accuracy

High dimensional accuracy of components built in MLAM can effectively improve feedstock utilization and reduce post-processing costs. Besides, surface finish optimization is an effective way to improve the fatigue performance of components since the valley of the local rough surface can boost cracks generation and propagation during stress loading [91,92]. Generally, the dimensional accuracy of components depends on process parameters and raw materials. The dimensional accuracy is typically better in LPBF than in LDED due to the smaller molten pool size [93]. Components fabricated in MLAM usually have higher dimensional accuracy since finer powders or thinner wires are used as feedstock [94,95].

Surface balling is a challenging issue in MLAM. The melted material forms solidified spherical particles on the layer surface after solidification, especially for powder feedstock [96]. Surface balling can be attributed to three main reasons, i.e., liquid phase shrinking into spheres due to excessive surface tension, poor wettability of molten particles, and partially melted powders sticking to components' surface during solidification. The balling phenomenon in LPBF results from excessive surface tension [97,98]. Besides, poor matching of process parameters significantly influences surface quality, such as over-melting and lack of fusion. It is worth noting that plasma plumes will be generated when the molten pool temperature reaches the evaporation point. The recoil pressure of the plasma plume causes spatters, deteriorating the layer bead surface quality (Fig. 12). Moreover, fluctuating bead morphology is easily produced by the molten pool oscillation resulting from plume excitation [99,100]. An insufficient protective atmosphere will lead to surface oxidation or stability deterioration of plasma ejection,

decreasing the forming quality [101].

Uneven materials deposition and thermal accumulation appear easily in some unique structures built by LDED, such as corners and crosses, leading to serious dimension deviation and low automation during deposition. When the feedstock feed speed or angle in LDED is unreasonable, the smooth transition of molten materials will be hindered. Especially in W-LDED, the wire may be melted at the edge of the laser beam to form a weak link liquid bridge, decreasing the forming quality of parts. Furthermore, the wire may collide with the abnormal hump of unique structures during deposition, resulting in a process termination [102,103].

The temperature change rate in the molten pool acted by laser can reach $10^2\text{--}10^4 \text{ K/s}$, inevitably leading to large residual stress [104,105]. During the sequential deposition process, the deformation of components will be created due to the accumulative residual stress. As the local residual stress exceeds the yield strength of the materials, some fatal defects appear, including delamination and cracking (Fig. 13) [106–108]. Thermal stress management strategies include optimizing the scanning path, controlling the dwelling time, or adding auxiliary thermal fields [109,110].

3.2. Internal defects

Different from dimension deviation, internal defects significantly deteriorate the mechanical properties of parts. The diagnosis of internal defects is a challenging issue. Components with unidentified internal defects have huge potential risks in engineering applications [111,112]. Internal defects of parts in MLAM mainly include pores and microcracks.

Pores are the most common defect in laser processing and have many inducing factors. Similar to the laser welding process, there is a "keyhole effect" in MLAM, i.e., a cavity in the molten pool after metal evaporation. The molten pool captures bubbles introduced by the keyhole collapse to form pores during the molten pool solidification process [113,114]. Lack of fusion will appear due to low heat input or a small overlap ratio between adjacent beads. Fig. 14 exhibits the schematic diagram of the lack-of-fusion defect and the relationship between pores and process parameters in LPBF [115,116]. For alloy materials, when the alloy elements evaporate, gas is easily captured by the molten pool to produce pores due to the fluid flow caused by the Marangoni force [117]. In LDED, the droplet transition causes turbulence on the molten pool surface, and the gas is involved in the fluid to form porosity flaws [118]. Moreover, poor feedstock properties, such as moisture and oxidation, can contaminate the molten pool and induce porosities or inclusions [119,120].

Internal cracks are often related to material properties and stress distribution. Metal materials with a high cracking tendency pose

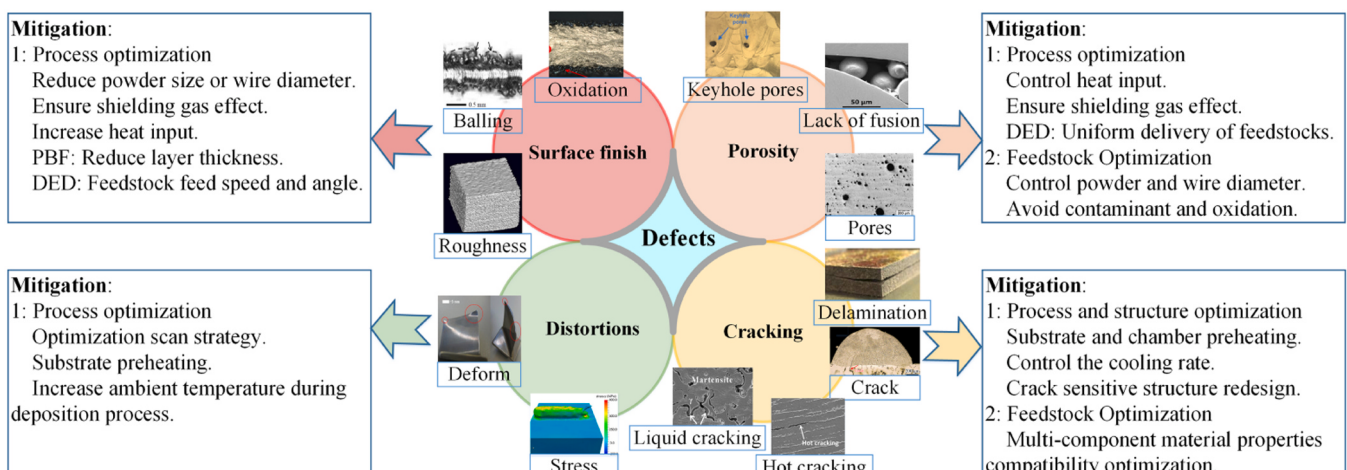


Fig. 11. Defects and corresponding mitigation methods in MLAM.

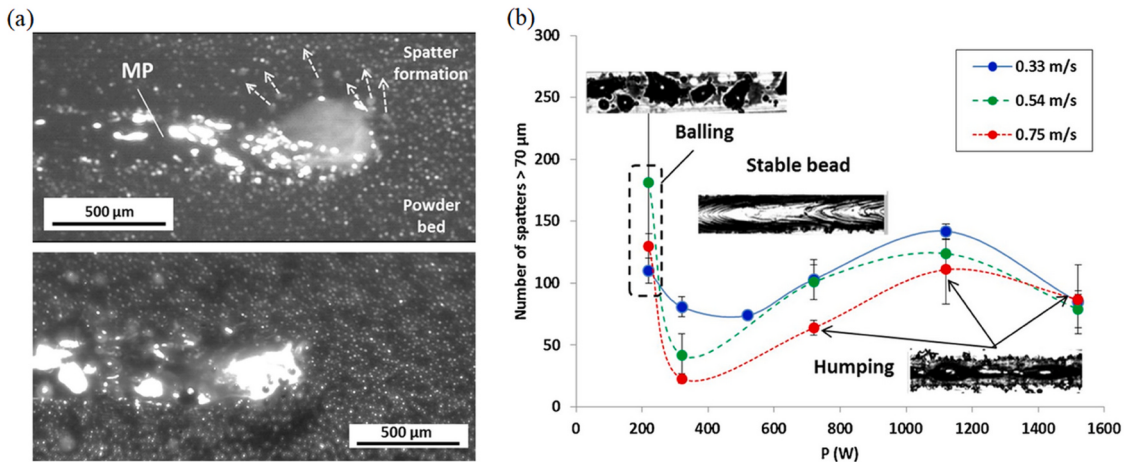


Fig. 12. (a) Typical molten pool morphology and spatters in LPBF. (b) Influence of process parameters on bead morphology [99].

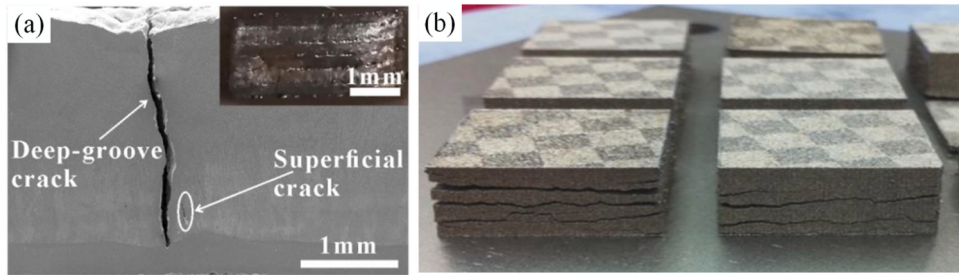


Fig. 13. (a) Surface cracks of Ni-Co-Mn-Al alloys in LDED [108]. (b) Layer delamination and cracking of M2 High-Speed Steel in LPBF [109].

considerable challenges to manufacturing [121]. In particular, the metallurgical bonding properties of dissimilar materials should be considered to prepare gradient structures in MLAM. From the metallurgy perspective, the crack types occurring in components mainly include solidification and liquation cracks [122,123]. Solidification cracks appear in the liquid film that finally solidifies at the grain boundary under the action of shrinkage stress. During deposition, the low melting eutectic is melted by the thermal cycle, inducing local cracking under stress to form liquation cracks. Generally, the residual stress concentrates on inter-layer areas or structural tips. Crack defects will erupt when the peak of residual stress exceeds the strength limit in these areas [124,125]. Improving residual stress distribution is a principal measure to mitigate crack defects.

3.3. Section summary

The surface defects in MLAM can be categorized as oxidation, balling, and deformation. The internal defects are mainly pores and cracks. Factors, including inappropriate process parameters, unstable protective atmosphere, and feedstock contamination, may induce these defects. Defect control in MLAM is systematic engineering. A single defect is usually subject to multiple process parameters. The control strategy of defects involves intricate multi-factor decoupling. The controllable parameters involved in MLAM are listed in Table 2. Selecting appropriate process parameters can save many process exploration costs.

4. Process control in MLAM

As a critical step in MLAM automation, process control is exposed to opportunities and challenges in the context of the rapid development of sensing techniques and data processing capabilities. Although many commercial MLAM systems have been developed, the building processes

still depend on human involvement, relying on operators' knowledge and experience. Therefore, developing an intelligent system is crucial for improving the automation level of MLAM.

Many control strategies have been used to achieve process feedback control in MLAM, including predictive control, repetitive control, and adaptive learning control [126]. Table 3 summarizes the monitoring objects and the process control strategies in MLAM. In recent years, the application potential of ML algorithms in MLAM process control has been discussed. Moreover, ML methods will become the development basis of intelligent control systems in MLAM with perception, learning, and self-evolution capacities [127,128].

4.1. Process control framework

In the early stage of process control, open-loop control strategies, in which the adjustment of process parameters depends on the quality assessment status of periodic processes, possess the characteristics of low efficiency and accuracy. Subsequently, automatic process control (APC) techniques, which can continuously compensate for deviations by dynamic feedback, have received wide attention. APC techniques markedly improve manufacturing efficiency and accuracy [129].

Automatic control techniques have experienced two stages, including classic APC and modern APC. In classic APC control, the relationship between the input and output of the experimental system is concerned, and the transfer function of the experimental system is established. This control strategy can only handle the single-input single-output system with deterministic models and is always difficult to reach the optimal control. Fig. 15 shows a schematic diagram of the classic feedback control system. In modern APC control, one of the breakthroughs is using state space equations to replace the transfer function. The experimental system analysis is performed in the time domain, which can expand the application object to a nonlinear, multi-

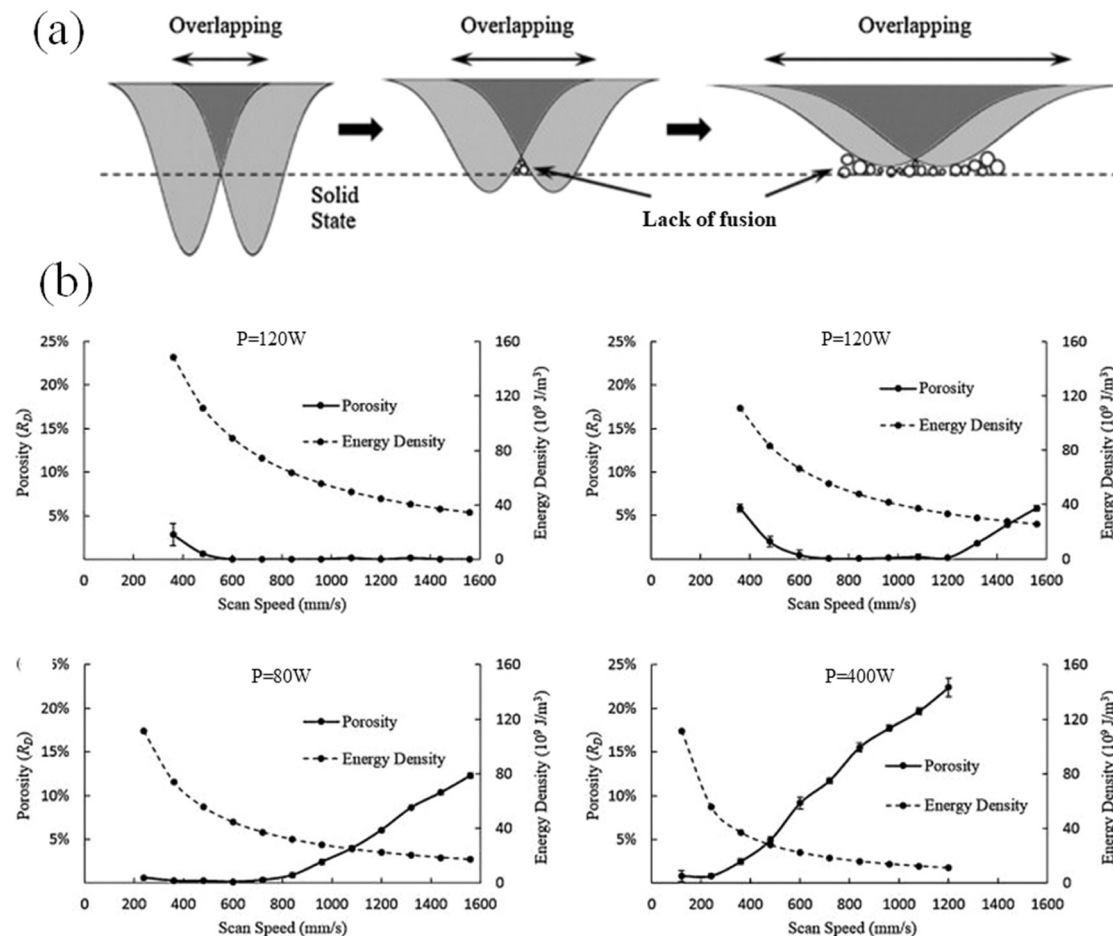


Fig. 14. (a) Schematic diagram of lack of fusion defects in LPBF. (b) Relationships between pores and process parameters [115].

Table 2
Controllable parameters in metal-based laser additive manufacturing.

Item	LPBF	P-LDED	W-LDED
Laser power	✓	✓	✓
Laser output mode	✓	✓	✓
Travel speed	✓	✓	✓
Powder feed rates		✓	
Wire feed speed			✓
Layer thickness	✓		
Shielding gas flow rate		✓	✓
Scan pattern & direction	✓	✓	✓
Spot size	✓	✓	✓
Powder size	✓	✓	
Wire diameter			✓
Chamber gas	✓		

variable, and time-varying system. Modern control includes linear system theory, dynamic system identification, best estimation theory, optimal control, and adaptive control.

Intelligent control combines control theory and artificial intelligence flexibly and can deal with uncertainties and complexities in the system. The controller design determines the system's response speed, adjustment accuracy, and adaptability [130]. The most widely used intelligent controllers include expert systems, fuzzy logic, neural networks, and biological intelligence search algorithms. ML algorithms based on data-driven can automatically establish and continuously optimize data dependence models. Therefore, the models' performances are significantly related to the amount and typicalness of the training data [131]. Fig. 16 shows a block diagram of the ML-based process control strategy

in MLAM. The prepared training data is used to train the ML model, and the process data is used to evolve the model during manufacturing and predict the optimal process parameters [132,133].

The main tasks of ML are to achieve classification, regression, and clustering by various algorithms. Typical ML algorithms are generally divided into four categories: supervised, semi-supervised, unsupervised, and reinforcement learning [134,135]. Fig. 16 displays the specific classification of various algorithms. ML algorithms can also extract and process in-depth features of collected data to provide optimal solutions for quality issues. However, the current applications of ML in process control are exposed to some challenges. Moreover, the data acquisition costs should be considered due to the enormous data required for training models. A large amount of computation is another limitation. The system's real-time performance will degrade due to the time-consuming calculation process [136,137]. Therefore, developing ML algorithms with high computational speed and low data dependence is necessary.

4.2. Current state-of-the-art

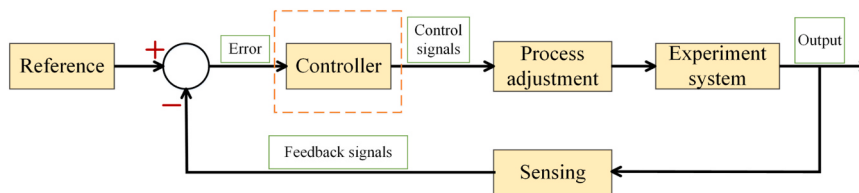
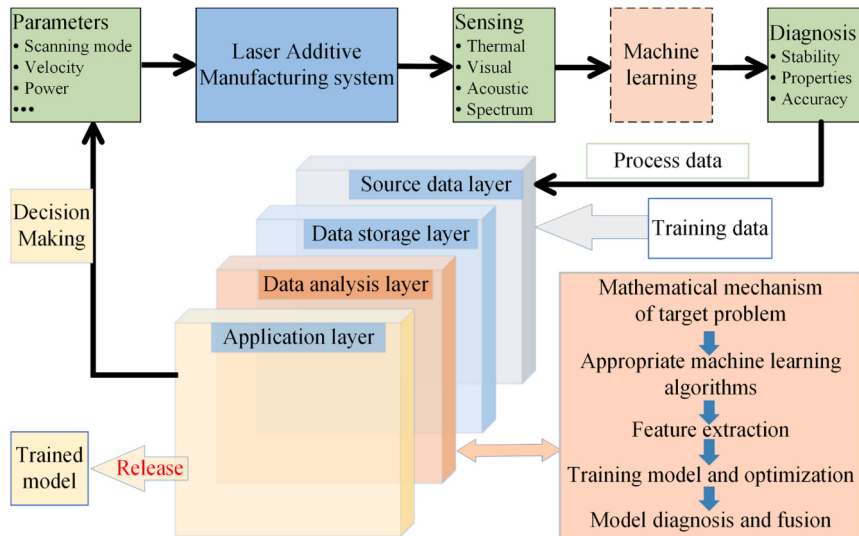
4.2.1. Laser powder bed fusion

Compared with LDED, LPBF, without the material feeding mechanism, possesses a more stable manufacturing process. However, maintaining the thermal state's consistency in the travel path of parts is difficult, especially for some unique structures sensitive to heat accumulation, such as sharp areas and overhanging structures. Currently, controlling parameters in LPBF concentrate on the laser power and the scanning mode. Limited by the manufacturing environment, thermal and visual sensing are the commonly used monitoring methods for

Table 3

Summary of process control research in MLAM.

Process	Control object	Sensing equipment	Adjusted parameter	Control strategy	Literature
LPBF	Geometry accuracy	Infrared camera	Laser power	PID	[138]
LPBF	Microstructure and microhardness	Pyrometer	Laser power	Sliding mode control	[140]
LPBF	Bead area	Digital camera	Laser power	Nonlinear inverse-dynamics control	[145]
LPBF	Uneven performance	Infrared camera	Scanning mode	Multi-input neural network feedback control	[150]
P-LDED	Layer width	Infrared camera	Laser power	PID	[151]
P-LDED	Layer width	CMOS camera	Laser power	Discrete control filter control	[159]
P-LDED	Layer height	CCD camera	Travel speed	Adaptive sliding mode control	[160]
P-LDED	Layer height	CCD camera	Travel speed	ANFIS control	[162]
P-LDED	Cooling rates	Infrared camera	Travel speed	PID	[167]
W-LDED	Geometry accuracy	Infrared camera	Laser power & Travel speed & Wire Feed speed	Combination controller	[173]
W-LDED	Dilution	Pyrometer	Laser power	PID	[174]
W-LDED	Geometry accuracy	Resistance sensor	Wire feed speed	Second-order iterative learning control	[178]
W-LDED	Geometry accuracy	Force sensor	Wire feed speed	Two-point controller	[179]
W-LDED	Layer height	3D scanner	Wire feed speed	Iterative learning control	[180]

**Fig. 15.** Schematic diagram of a feedback control system.**Fig. 16.** Block diagram of ML-based process control strategy in MLAM.

process control in LPBF. Thermal and visual signals can characterize the forming quality, microstructure, and properties of parts [138–141]. For instance, Rezaeifar et al. [140] proposed to control the laser power to obtain a stable molten pool temperature for more uniform microstructures and higher mechanical properties of deposited parts. Tristan et al. [141] used an inline coherent imaging (ICI) method to extract the area features of protrusions and depressions in each layer and utilized a pulsed laser to ablate or refill the location with large height deviations to achieve in-situ correction. The surface roughnesses of the samples can

decrease by 54%.

Numerical simulation based on mathematical models can precisely predict and depict the actual evolution of the physical process. Using the calculation results as the input data of the control system is a novel scheme to improve the qualities of components in LPBF [142,143]. Wang et al. [144] established a closed-loop control framework based on a finite element model (FEM). The calculated molten pool width was fed into the proportional-integral (PI) controller to adjust the laser power. The core concept of the control framework was using the output signals

collected from the FEM to update the control signals sent back to the model step by step (Fig. 18). Wang et al. [145] constructed a numerical simulation model to calculate the molten pool dynamics during laser beam scanning. They used the calculated cross-sectional area of the molten pool as a feedforward signal of the nonlinear inverse dynamic controller to regulate the laser power. This strategy can stabilize the heat input to suppress the keyhole or over-melting. Syed et al. [146] established a thermal effect model between adjacent beads to describe the laws of thermal interference from adjacent beads. The molten pool size of the current bead inferred from the model was used as the input signal of the proportional integral derivative (PID) controller to regulate the laser power for improving the molten pool stability.

ML algorithms can understand the manufacturing state of the previous step and implement decision-making in the subsequent step [147, 148]. Francis et al. [149] proposed a deep reinforcement learning framework to intuitively learn the influences of process parameters on heat accumulation. The framework can determine the heat accumulation area and maintain uniform molten pool depth by regulating the laser power or the scanning speed. Zhong et al. [150] introduced a multi-input neural network to establish a control model to analyze the complex thermal history in LPBF. As illustrated in Fig. 19, the overall sintering state was evaluated by the process characteristics and thermal histories, and the next layer's laser power was further adjusted by a PID controller to realize the on-line compensation of the heat accumulation difference.

4.2.2. Powder-based laser direct energy deposition

Compared with LPBF, LDED is a near-net shaping technique with higher efficiency. Many studies have been done on the process feedback control in LDED and mainly focus on thermal state and geometric control methodologies of deposited parts [151,152]. Various controlling variables can be adjusted to optimize the part qualities, including laser power, scanning speed, powder feed speed, laser defocusing, and powder focal spot position [153–158].

Visual sensing is the most common method in the feedback control system to monitor bead geometries [159]. Zeinali et al. [160] used a CCD camera to monitor the cladding layer height and proposed a sliding mode controller to adjust the travel speed to realize a more uniform layer height during sequential depositions. Meysam et al. [161] designed a layer-dependent adaptive PI controller to control the molten pool width by adjusting the laser power. This controller overcomes the dynamic response changes in the controller parameters in different deposition layers. Mohammad et al. [162] used a CCD camera to monitor the layer height and designed a neuro-fuzzy model controller to regulate the travel speed to achieve a uniform layer height. In addition, thermal sensing devices, such as pyrometers [163] and IR cameras [164], exhibit excellent capacities for extracting the temperatures and sizes of the molten pool. Temperature deviations of the molten pool in

LDED are significant due to heat accumulation [165]. Increasing the inter-layer dwell time and regulating the molten pool's cooling rate can optimize the microstructure and mechanical properties of as-built parts [166]. As described by Mohammad et al. [167], an IR camera was used to monitor the dynamic changes in the molten pool temperature, and the cooling rate was taken as the PID controller input to regulate the travel speed. Fig. 20 shows the travel speed variations at a fixed cooling rate. The microstructure and hardness of the samples fabricated under the closed-loop control were more uniform. After applying the closed-loop control of molten pool temperatures in LDED, the as-built parts' corrosion resistance improved, and the porosity decreased markedly [168].

Multi-signal cooperative monitoring can analyze the dynamic change of the manufacturing system systematically. Tyralla et al. [169] utilized a laser-line triangulation sensor and a thermal camera to monitor the layer height and the molten pool temperature, respectively. A dual-loop PID control strategy, which controlled the overlap rate and the height deviation simultaneously, was designed to achieve multi-parameter adjustment, including the laser power and the lateral movement distance of the processing head. Based on the dual-loop control strategy, two PI controllers were used to control the molten pool temperature and deposition height cooperatively, and the laser power was chosen as the only regulating parameter [170]. The results showed that this method could effectively improve the dimensional accuracy and the thermal behavior uniformity of parts in P-LDED.

4.2.3. Wire-based laser direct energy deposition

Control strategies for dimensional accuracy of parts built in W-LDED and P-LDED show similarities. To fulfill quality requirements, geometric sizes or temperature deviations were taken as the feedback signals of the closed-loop control system to regulate the process parameters [171–174]. For instance, Almir et al. [175] designed a control system combining a feedforward compensator and a feedback PI controller to achieve the stable control of bead heights and widths monitored by a double visual sensing system. Garmendia et al. [176] used a linear controller to adjust the wire feed speed based on the height deviation of the local position from the average layer height and developed an intra-layer adaptive trajectory planning strategy to correct height fluctuations. Besides, many control strategies have been proposed in W-LDED based on special sensing methods, such as resistance and force sensing.

In general, the bridging transition mode of droplets improves part qualities in W-LDED [177]. There is a current loop between the substrate and the wire when an appropriate voltage is applied. The molten pool's resistance can be calculated by monitoring the voltage and current between the wire nozzle and the substrate. Based on this principle, Hagqvist et al. [178] used the resistance between the nozzle and the substrate as a feedback signal and developed an iterative learning controller to regulate the wire feed speed for improving the forming

Machine Learning Techniques			
Supervised	Semi-supervised	Reinforced	Unsupervised
<ul style="list-style-type: none"> • Naives bayes • Decision tree • Support vector machine • Genetic programming • Radial basis function • Particle swarm algorithm • Artificial nerual network • Siamese neural network • Long short term memory • Convolution neural network 	<ul style="list-style-type: none"> • Gaussian mixture • Generative models • Graph-based methods • Model low-density separation 	<ul style="list-style-type: none"> • Q-learning • Temporal difference • Deep adversarial network 	<ul style="list-style-type: none"> • K means clustering • Self-organising map • Restricted Boltzmann machine

Fig. 17. Classification of ML algorithms.

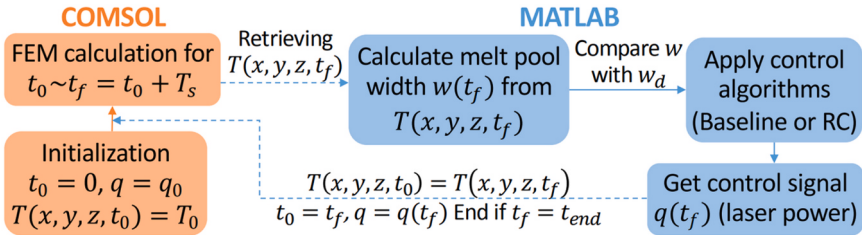


Fig. 18. Schematic diagram of proposed simulation-based closed-loop system [144].

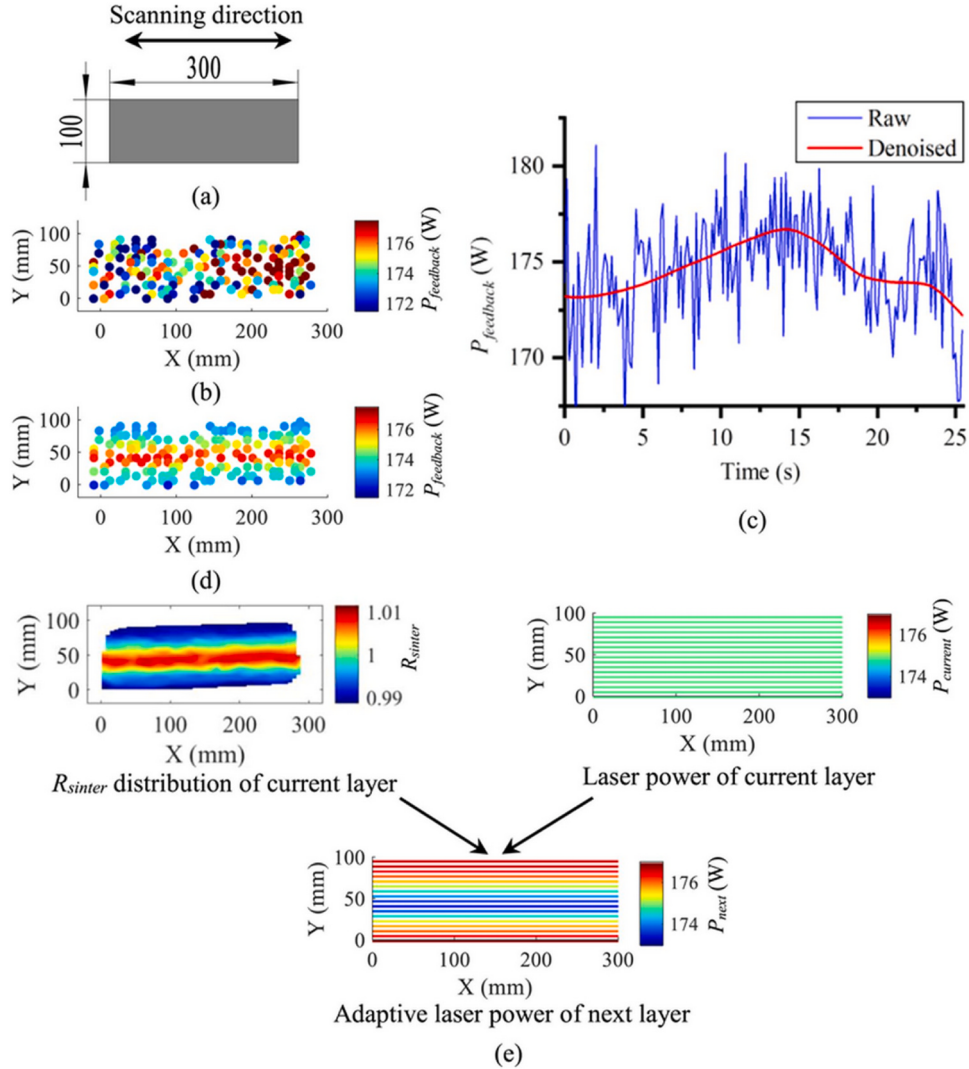


Fig. 19. Adaptive laser power calculation process [150].

quality of deposited layers. Teichmann et al. [179] developed a two-point controller to regulate the force between the wire and the molten pool by a force-controlled wire feeder for improving the droplet transition stability in LDED. The force-controlled wire feeder consisted of two blocks. One was fixed to the LDED system, and the other was floating. The displacement between both blocks was converted to a force applied to the wire feeder by a force sensor. Repairing the size deviations from previously deposited layers is crucial for quality assurance [180].

4.3. Section summary

The literature reviewed above mainly focuses on dimensional

accuracy in MLAM. Research on internal defect control needs to be more comprehensive. Feedback signals in process control mainly include visual and thermal signals that can characterize layer characteristics, such as layer widths, layer heights, and temperatures. Many advanced control strategies have been applied in MLAM, including predictive, adaptive, and model-based control. However, the PID controller, with the advantage of a simple debugging process, is still popular for process control in MLAM. Currently, ML algorithms have been widely used for the diagnosis and classification of defects. However, the application of ML algorithms in closed-loop control is still limited due to the relatively immature framework of end-to-end learning and insufficient training data.

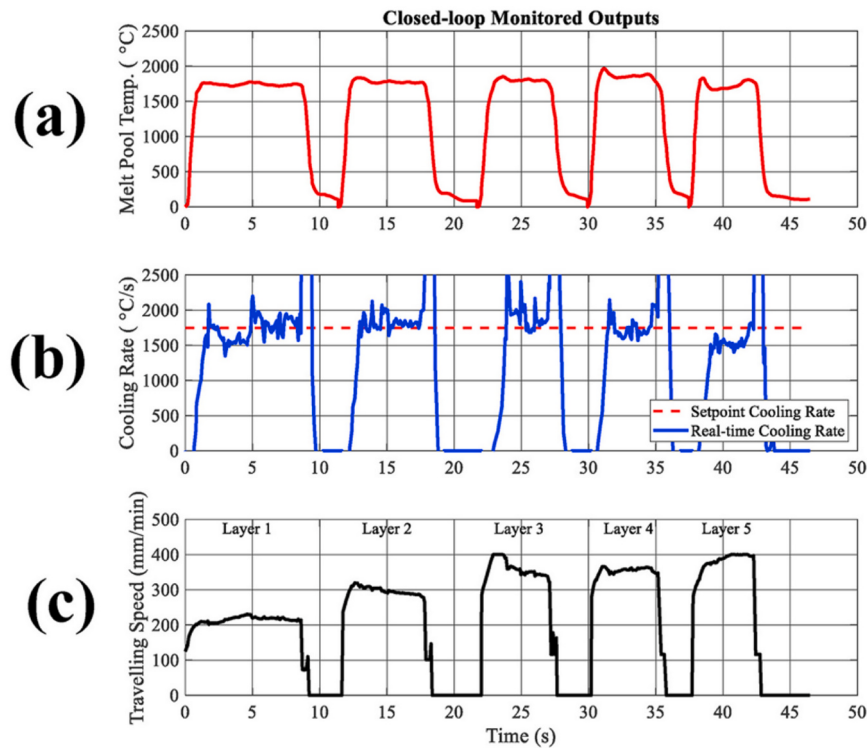


Fig. 20. Molten pool temperature and travel speed evolutions as the cooling rate controlled at 1750 °C/s [167].

5. Conclusion

Monitoring and control are two indispensable parts of process closed-loop control to tackle the low robustness and repeatability in MLAM. As shown in Fig. 21, the relationships among the above sections are similar to the ancient Chinese Tai Chi map. Both parts must be developed in coordination to promote the progress of MLAM automation. This field has high research value and plays a crucial role in breaking through the industry application limits of MLAM. This research carries out a comprehensive review of previous studies on in-situ monitoring and process control in MLAM. The characteristics and limitations of various sensing systems applied in MLAM are analyzed. Defects in MLAM are categorized, and the corresponding induction mechanisms and mitigation measures are discussed. The development of the process control framework is reviewed. The research efforts are categorized based on sensing methods, controller types, and controlled objects.

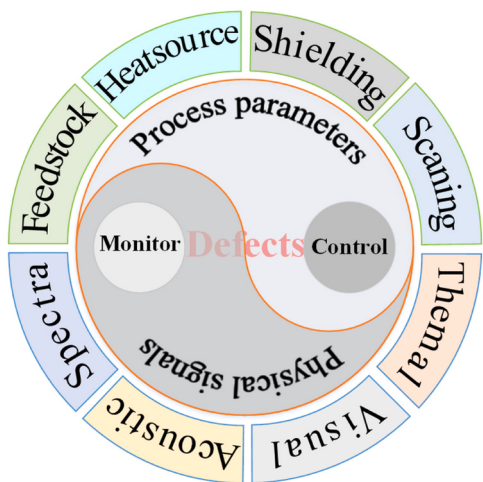


Fig. 21. Schematic diagram of the relationship among the above sections.

6. Future outlooks

6.1. Process monitoring

Currently, many mature systems monitor single geometrical features of beads in MLAM. However, establishing synchronous sensing systems to monitor various features in MLAM is rarely involved. The priority should be given to clarifying the complex coupling effects among various signals in MLAM for developing multi-sensor synchronous sensing techniques since the mutual interference among different signals leads to many uncertainties. Moreover, multi-information sensing requires robust data transmission performance. It is necessary to introduce data transmission technologies with low latency to ensure the multi-sensor system's performance, for example, 5 G techniques. Besides, soft sensors based on ML or numerical calculation can obtain information challenging to measure in MLAM, such as microstructure and thermal evolution characteristics, significantly reducing the sensing device costs. Therefore, enhancing research investment of soft-sensors is valuable.

Different factors influence internal defects in as-built components due to the nonlinearity, strong coupling, and multi-parameter characteristics in MLAM. Depending on single sensing information to diagnose internal defects is unreliable. Although using AE sensing to characterize internal defect states has achieved a good effect in the laboratory, this method needs to improve its robustness and is prone to gaining distorted information in actual industrial sites. Developing multi-information fusion algorithms or fusion models based on multi-sensor systems is necessary to achieve higher accuracy and stronger robustness in defect monitoring.

6.2. Process control

Many advanced monitoring technologies, such as AE sensing and ML-assisted visual or thermal sensing, are yet to be integrated into the closed-loop control system in MLAM, meaning that many development studies are needed. The single variable control in MLAM, such as molten

pool width or layer height, has achieved significant results. However, regulating a single process parameter will affect other geometrical features due to the coupling effect. Therefore, developing multi-variable control systems is the only way to improve the intelligence level of MLAM. Besides, ML exhibits excellent potential in the control field for nonlinear multi-input multi-output systems subjected to state constraints. Extracting unknown relationships between process parameters and geometrical features based on ML algorithms is practicable. On this basis, it is possible to establish a controller through end-to-end interactive training directly.

6.3. Performance of ML models

ML has been widely applied to classify or predict layer features in MLAM. However, high-performance ML models rely on high-quality training data and label mapping. Large-scale dataset acquisition and model training are complex and costly. Therefore, the main development directions for ML are to reduce the dependence on training data volume and improve computational efficiency. Furthermore, the training data range limits the cognitive ability of current ML models, meaning that handling events beyond the training data range may lead to uncertainties in predictive results. Therefore, improving the generalization ability of ML models to release their application potential in MLAM has great significance.

Declaration of Competing Interest

We would like to submit the enclosed manuscript entitled “A review of in-situ monitoring and process control system in metal-based laser additive manufacturing”, which we wish to be considered for publication in “Journal of manufacturing systems”. This paper is original. Neither the entire paper nor any part of its content has been published or has been accepted elsewhere. We declare that we do not have any commercial or associative interest that represents a conflict of interest in connection with the work submitted.

Acknowledgements

This work was funded by National Natural Science Foundation of China, no. 62173280 and no. 51975491, Sichuan Science and Technology Program, no. 2023NSFSC1956, State Key Lab of Advanced Welding and Joining, Harbin Institute of Technology, no. AWJ-21M18, and the Fundamental Research Funds for the Central Universities, no. 2682023ZTPY023. All the cited figures and tables in the review paper are cited in the reference. If there is any copyright omission, please contact the author for deletion.

References

- [1] Steen WM, Mazumder J. *Laser Material Processing*. Berlin, Germany: Springer.; 2010.
- [2] Xiong J, Wen C. Arc plasma, droplet, and forming behaviors in bypass wire arc-directed energy deposition. *Addit Manuf* 2023;70:103558.
- [3] Liu ZY, Zhao DD, Wang P, Yan M, Yang C, Chen ZW, Lu J, Lu Z. Additive manufacturing of metals: Microstructure evolution and multistage control. *J Mater Sci Technol* 2022;100:224–36.
- [4] Gao C, Sarah W, Wang SR. Eco-friendly additive manufacturing of metals: Energy efficiency and life cycle analysis. *J Manuf Syst* 2021;60:459–72.
- [5] Byron BM, Paul G, Glen S, Michael B, Jean P, Elena L, Martin L, Filippo B, Anton DP. Metal additive manufacturing in aerospace: A review. *Mater Des* 2021;109:110008.
- [6] Davoud J, Tom HJ, Vaneker IG. Wire and arc additive manufacturing: Opportunities and challenges to control the quality and accuracy of manufactured parts. *Mater Des* 2021;202:109471.
- [7] Mostafaei A, Ghaasiaan R, Ho IT, Strayer S, Chang KC, Shamsaei N, Shao S, Paul S, Yeh AC, Tin S. To A. Additive manufacturing of nickel-based superalloys: A state-of-the-art review on process-structure-defect-property relationship. *Prog Mater Sci* 2023;136:101108.
- [8] Davoud J, Koen JH, Bernard JG, Wessel W, Laura CG, Tom HJV, Naveed UR, Gert WR, Ian G. Porous materials additively manufactured at low energy: Single-layer manufacturing and characterization. *Mater Des* 2020;191:108654.
- [9] Tan C, Li R, Su J, Du D, Du Y, Attard B, Chew Y, Zhang H, Lavernia EJ, Faurelle Y, Teng J, Dong A. Review on field assisted metal additive manufacturing. *Int J Mach Tools Manuf* 2023;189:104032.
- [10] Jerard VG, Sneha PN, Ross WC, Liu H, Chen H, Robert MS, Jack LB, Anthony DR. Defect structure process maps for laser powder bed fusion additive manufacturing. *Addit Manuf* 2020;36:101552.
- [11] Ramírez IS, Marquez FPG, Papaelias M. Review on additive manufacturing and non-destructive testing. *J Manuf Syst* 2023;66:260–86.
- [12] AbouelNour Y, Gupta N. In-situ monitoring of sub-surface and internal defects in additive manufacturing: A review. *Mater Des* 2022;222:111063.
- [13] Wang B, Hu SJ, Sun L, Freiheit T. Intelligent welding system technologies: state-of-the-art review and perspectives. *J Manuf Syst* 2020;56:373–91.
- [14] Xi X, Lin D, Song X, Luo X, Ma R, Shi Z, Bian H, Fu W, Dong Z, Tan C. Strength-plasticity transition mechanism after the solution treatment of GH3230 superalloy fabricated via laser powder bed fusion. *Mater Sci Eng A* 2023;876:145124.
- [15] Xia C, Pan Z, Polden J, Li H, Xu Y, Chen S, Zhang Y. A review on wire arc additive manufacturing: Monitoring, control and a framework of automated system. *J Manuf Syst* 2020;57:31–45.
- [16] Ronan MC, Muhammed AO, Cian H, Eanna MC, Darragh SE, Vijayaraghavan RK, Joshi AM, Garzon VA, Dowling DP, McNally PJ, Brabazon D. In-situ sensing, process monitoring and machine control in Laser Powder Bed Fusion: A Rev Addit Manuf 2021;45:102058.
- [17] Cai W, Wang JZ, Jiang P, Cao LC, Mi GY, Zhou Q. Application of sensing techniques and artificial intelligence-based methods to laser welding real-time monitoring: A critical review of recent literature. *J Manuf Syst* 2020;57:1–18.
- [18] Lin X, Zhu K, Fuh JYH, Duan X. Metal-based additive manufacturing condition monitoring methods: From measurement to control. *ISA Trans* 2022;120:147–66.
- [19] Oliveira JP, Santos TG, Miranda RM. Revisiting fundamental welding concepts to improve additive manufacturing: From theory to practice. *Prog Mater Sci* 2020;107:100590.
- [20] Rajaram NM, Nallusamy S. Experimental analysis of aluminum alloy metal matrix composite with tungsten carbide by an in-situ method using sem. *Rasayan J Chem* 2018;11(1):355–60.
- [21] Mahmood MA, Alabtah FG, Yasser A, Khraisheh M. On the laser additive manufacturing of high-entropy alloys: A critical assessment of in-situ monitoring techniques and their suitability. *Mater Des* 2023;226:111658.
- [22] Jafari-Marandi R, Khanzadeh M, Tian W, Smith B, Bian L. From in-situ monitoring toward high-throughput process control: cost-driven decision-making framework for laser-based additive manufacturing. *J Manuf Syst* 2019;51:29–41.
- [23] Tang Z, Liu W, Wang Y, Saleheen KM, Liu Z, Peng S, Zhang Z, Zhang H. A review on in situ monitoring technology for directed energy deposition of metals. *Int J Adv Manuf Technol* 2020;108:3437–63.
- [24] Li Y, Xiao W, Xiao H, Liu X, He K, Xie P, Song L. Enhanced molten-pool boundary stability for microstructure control using quasi-continuous-wave laser additive manufacturing. *J Mater Res Technol* 2023;23:238–44.
- [25] Mazzarisi M, Angelastro A, Latte M, Colucci T, Palano F, Campanelli SL. Thermal monitoring of laser metal deposition strategies using infrared thermography. *J Manuf Process* 2023;85:594–611.
- [26] Kim S, Jeon I, Sohn H. Infrared thermographic imaging based real-time layer height estimation during directed energy deposition. *Opt Lasers Eng* 2023;168:107661.
- [27] Chandrasekar S, Coble III JB, FL, Carver K, Beauchamp S, Godfrey A, Paquit V, Babu SS. Similarity analysis for thermal signature comparison in metal additive manufacturing. *Mater Des* 2022;224:111261.
- [28] Kayacan MY, Yilmaz N. An investigation on the measurement of instantaneous temperatures in laser assisted additive manufacturing by thermal images. *Measurement* 2020;160:107825.
- [29] Marshall GJ, Thompson SM, Shamsaei N. Data indicating temperature response of Ti-6Al-4V thin-walled structure during its additive manufacture via Laser Engineered Net Shaping. *Data Brief* 2016;7:697–703.
- [30] Marshall GJ, Young WJ, Scott MT, Nima S, Steve RD, Shao S. Understanding the microstructure formation of Ti-6Al-4V during direct laser deposition via in-situ thermal monitoring. *Jom* 2016;68:778–90.
- [31] Vallabh CKP, Zhao X. Melt pool temperature measurement and monitoring during laser powder bed fusion based additive manufacturing via single-camera two-wavelength imaging pyrometry (STWIP). *J Manuf Process* 2022;79:486–500.
- [32] Zheng L, Zhang Q, Cao H, Wu W, Ma H, Ding X, Yang J, Duan X, Fan S. Melt pool boundary extraction and its width prediction from infrared images in selective laser melting. *Mater Des* 2019;183:108110.
- [33] Khanzadeh M, Chowdhury S, Marufuzzaman M, Tschopp MA, Bian L. Porosity prediction: Supervised-learning of thermal history for direct laser Deposition. *J Manuf Syst* 2018;47:69–82.
- [34] Demir AG, Giorgi CD, Previtali B. Design and Implementation of a Multisensor Coaxial Monitoring System with Correction Strategies for Selective Laser Melting of a Maraging Steel. *J Manuf Sci Eng* 2018;140:041003.
- [35] Mitchell JA, Thomas AI, Daryl D, Jonathan DM, Jared B. Linking pyrometry to porosity in additively manufactured metals. *Addit Manuf* 2020;31:100946.
- [36] Wei J, He Y, Wang F, He Y, Rong X, Chen M, Wang Y, Yue H, Liu J. Convolutional neural network assisted infrared imaging technology: An enhanced online processing state monitoring method for laser powder bed fusion. *Infrared Phys Technol* 2023;131:104661.
- [37] Hu Y, Chen H, Liang X, Xie J. Monitoring molten pool temperature, grain size and molten pool plasma with integrated area of the spectrum during laser additive manufacturing. *J Manuf Process* 2021;64:851–60.

- [38] Devesse W, Baere DD, Guillaume P. High resolution temperature measurement of liquid stainless steel using hyperspectral imaging. *Sensors* 2017;17:1253–60.
- [39] Liu Y, Guo L, Gao H, You Z, Ye Y, Zhang B. Machine vision based condition monitoring and fault diagnosis of machine tools using information from machined surface texture: A review. *Mech Syst Signal Process* 2022;164:108068.
- [40] Binega E, Yang L, Sohn H, Cheng JCP. Online geometry monitoring during directed energy deposition additive manufacturing using laser line scanning. *Precis Eng* 2022;73:104–14.
- [41] Pandiy V, Rita DD, Shevchik S, Masinelli G, Tri LQ, Logé R, Wasmer K. Deep transfer learning of additive manufacturing mechanisms across materials in metal-based laser powder bed fusion process. *J Mater Process Technol* 2022;303:117531.
- [42] Fu Y, Downey ARJ, Yuan L, Zhang T, Pratt A. Machine learning algorithms for defect detection in metal laser-based additive manufacturing: A review. *J Manuf Process* 2022;75:693–710.
- [43] Liu R, Yang H. Multimodal probabilistic modeling of melt pool geometry variations in additive manufacturing. *Addit Manuf* 2023;61:103375.
- [44] Le TN, Lee MH, Lin ZH, Tran HC, Lo YL. Vision-based in-situ monitoring system for melt-pool detection in laser powder bed fusion process. *J Manuf Process* 2021;68:1735–45.
- [45] Hsu HW, Lo YL, Lee MH. Vision-based inspection system for cladding height measurement in Direct Energy Deposition (DED). *Addit Manuf* 2019;27:371–8.
- [46] Mehrdad IT, Ehsan T. An image-based feature tracking algorithm for real-time measurement of clad height. *Mach Vis Appl* 2007;18:343–54.
- [47] Perani M, Baraldo S, Decker M, Vandone A, Valente A, Paoli B. Track geometry prediction for Laser Metal Deposition based on on-line artificial vision and deep neural networks. *Robot Comput Manuf* 2023;79:102445.
- [48] Fischer FG, Zimmermann MG, Praetzs N, Knaak C. Monitoring of the powder bed quality in metal additive manufacturing using deep transfer learning. *Mater Des* 2022;222:111029.
- [49] Snow Z, Scime L, Ziabari A, Fisher B, Paquit V. Observation of spatter-induced stochastic lack-of-fusion in laser powder bed fusion using in situ process monitoring. *Addit Manuf* 2023;61:103298.
- [50] Nael MA, Erty DS, Vlasea M, Fieghut P. Adaptive vision-based detection of laser-material interaction for directed energy deposition. *Addit Manuf* 2020;36:101468.
- [51] Sun Z, Guo W, Li L. In-process measurement of melt pool cross-sectional geometry and grain orientation in a laser directed energy deposition additive manufacturing process. *Opt Laser Technol* 2020;129:106208.
- [52] Kim J, Yang Z, Ko H, Cho H, Lu Y. Deep learning-based data registration of melt-pool-monitoring images for laser powder bed fusion additive manufacturing. *J Manuf Syst* 2023;68:117–29.
- [53] Palm MS, Diepold B, Neumeier S, Hoeppel HW, Goeken M, Zaeh MF. Detection and effects of lack of fusion defects in Hastelloy X manufactured by laser powder bed fusion. *Mater Des* 2023;230:111941.
- [54] Kanko JA, Sibley AP, Fraser JM. In situ morphology-based defect detection of selective laser melting through inline coherent imaging. *J Mater Process Technol* 2016;231:488–500.
- [55] Fischer FG, Birk N, Rooney L, Jauer L, Schleifenbaum JH. Optical process monitoring in Laser Powder Bed Fusion using a recoater-based line camera. *Addit Manuf* 2021;47:102218.
- [56] Chen L, Bi G, Yao X, Tan C, Su J, Ng NPH, Chew Y, Liu K, Moon SK. Multisensor fusion-based digital twin for localized quality prediction in robotic laser-directed energy deposition. *Robot Comput Manuf* 2023;84:102581.
- [57] Abdelrahman M, Reutzel EW, Nassar AR, Starr TL. Flaw detection in powder bed fusion using optical imaging. *Addit Manuf* 2017;15:1–11.
- [58] Scime L, Beuth J. Using machine learning to identify in-situ melt pool signatures indicative of flaw formation in a laser powder bed fusion additive manufacturing process. *Addit Manuf* 2019;25:151–65.
- [59] Wang K. Contrastive learning-based semantic segmentation for In-situ stratified defect detection in additive manufacturing. *J Manuf Syst* 2023;68:465–76.
- [60] Mozaffari A, Fathi A, Khajepour A, Toyserkani E. Optimal design of laser solid freeform fabrication system and real-time prediction of melt pool geometry using intelligent evolutionary algorithms. *Appl Soft Comput* 2013;13:1505–19.
- [61] Tempelman JR, Wachtor AJ, Flynn EB, Depond PJ, Forien JB, Guss GM, Calta NP, Matthews MJ. Detection of keyhole pore formations in laser powder-bed fusion using acoustic process monitoring measurements. *Addit Manuf* 2022;55:102735.
- [62] Tempelman JR, Wachtor AJ, Flynn EB, Depond PJ, Forien JB, Guss GM, Calta NP, Matthews MJ. Sensor fusion of pyrometry and acoustic measurements for localized keyhole pore identification in laser powder bed fusion. *J Mater Process Technol* 2022;308:117656.
- [63] Plotnikov Y, Henkel D, Burdick J, French A, Sions J, Bourne K. Infrared-assisted acoustic emission process monitoring for additive manufacturing. *AIP Conf Proc* 2019;2102:020006.
- [64] Gutknecht K, Cloots M, Sommerhuber R, Wegener K. Mutual comparison of acoustic, pyrometric and thermographic laser powder bed fusion monitoring. *Mater Des* 2021;210:110036.
- [65] Chen L, Yao X, Tan C, He W, Su J, Weng F, Chew Y, Ng NPH, Moon SK. In-situ crack and keyhole pore detection in laser directed energy deposition through acoustic signal and deep learning. *Addit Manuf* 2023;69:103547.
- [66] Nallusamy S, Sujatha K. Experimental analysis of nanoparticles with cobalt oxide synthesized by coprecipitation method on electrochemical biosensor using FTIR and TEM. *Mater Today: Proc* 2021;37:728–32.
- [67] Gaja H, Liou F. Defects monitoring of laser metal deposition using acoustic emission sensor. *Int J Adv Manuf Technol* 2017;90:561–74.
- [68] Li K, Li T, Ma M, Wang D, Deng W, Lu H. Laser cladding state recognition and crack defect diagnosis by acoustic emission signal and neural network. *Opt Laser Technol* 2021;142:107161.
- [69] Ito K, Kusano M, Demura M, Watanabe M. Detection and location of microdefects during selective laser melting by wireless acoustic emission measurement. *Addit Manuf* 2021;40:101915.
- [70] Kononenko DY, Nikanova V, Seleznev M, Brink J, Chernyavsky D. An in situ crack detection approach in additive manufacturing based on acoustic emission and machine learning. *Addit Manuf Lett* 2023;5:100130.
- [71] Ye D, Zhang Y, Zhu K, Hong GK, Fuh YHJ. Characterization of acoustic signals during a direct metal laser sintering process. In: *Advances in Energy Science and Equipment Engineering II*. CRC Press; 2017. p. 1315–20.
- [72] Ye D, Hong GK, Zhang Y, Zhu K, Fuh YHJ. Defect detection in selective laser melting technology by acoustic signals with deep belief networks. *Int J Adv Manuf Technol* 2018;96:2791–801.
- [73] Pandiy V, Rita DD, Shevchik S, Masinelli G, Logé R, Wasmer K. Analysis of time, frequency and time-frequency domain features from acoustic emissions during Laser Powder-Bed fusion process. *Procedia CIRP* 2019;94:392–7.
- [74] Chen Y, Jiang L, Peng Y, Wang M, Xue Z, Wu J, Yang Y, Zhang J. Ultra-fast laser ultrasonic imaging method for online inspection of metal additive manufacturing. *Opt Lasers Eng* 2023;160:107244.
- [75] Allam A, Alfahami O, Patel H, Sugino C, Harding M, Ruzzene M, Erturk A. Ultrasonic testing of thick and thin Inconel 625 alloys manufactured by laser powder bed fusion. *Ultrasonics* 2022;125:106780.
- [76] Milon C, Vanhooye A, Obaton AF, Penot JD. Development of laser ultrasonics inspection for online monitoring of additive manufacturing. *Weld World* 2018;62:653–61.
- [77] Zhang J, Zhao X, Yang B, Li J, Liu Y, Ma G, Yuan S, Wu J. Nondestructive evaluation of porosity in additive manufacturing by laser ultrasonic surface wave. *Measurement* 2022;193:110944.
- [78] Dai T, Jia XJ, Zhang J, Wu JF, Sun YW, Yuan SX, Ma GB, Xiong XJ, Ding H. Laser ultrasonic testing for near-surface defects inspection of 316L stainless steel fabricated by laser powder bed fusion. *China Foundry* 2021;18:360–8.
- [79] Lv G, Yao Z, Chen D, Li Y, Cao H, Yin A, Liu Y, Guo S. Fast and high-resolution laser-ultrasonic imaging for visualizing subsurface defects in additive manufacturing components. *Mater Des* 2023;225:111454.
- [80] Huang Y, Zhang F, Yuan J, Jia C, Ren X, Yang L. Investigation on surface morphology and microstructure of double-wire + arc additive manufactured aluminum alloys based on spectral analysis. *J Manuf Process* 2022;84:639–51.
- [81] Shi Y, Zhao N, Chen Y, Liu J, Li J, Hou Z, Zhou G. Spectroscopic analysis of Nd/Al co-doped silica glass fabricated by laser additive manufacturing. *J Non-Cryst Solids* 2023;604:122139.
- [82] Song L, Mazumder J. In-situ spectroscopic analysis of laser induced plasma for monitoring of composition during direct metal deposition process. *International Congress on Applications of Lasers & Electro-Optics: Laser Inst Am* 2010;1:166–71.
- [83] Louqua CS, Escano LI, Qu M, Smith CC, Landers RG, Bristow DA, Chen L, Kinzel EC. In-situ optical emission spectroscopy of selective laser melting. *J Manuf Process* 2020;53:336–41.
- [84] Liu S, Liu W, Harrooni M, Ma J, Kovacevic R. Real-time monitoring of laser hot-wire cladding of Inconel 625. *Opt Laser Technol* 2014;62:124–34.
- [85] Dunbar AJ, Nassar AR. Assessment of optical emission analysis for inprocess monitoring of powder bed fusion additive manufacturing. *Virtual Phys Prototyp* 2017;13:14–9.
- [86] Mohammad M, Abdalla RN, Alexander JD, Prahalada R. In-Process Monitoring of Porosity in Additive Manufacturing using Optical Emission Spectroscopy. *IIE Trans* 2020;52:500–15.
- [87] Gong G, Ye J, Chi Y, Zhao Z, Wang Z, Xia G, Du X, Tian H, Yu H, Chen C. Research status of laser additive manufacturing for metal: a review. *J Mater Res Technol* 2021;15:855–84.
- [88] Cai Y, Luo Y, Zhang F, Peng Y, Yang T, Liu J. Study of the microstructure and mechanical properties in multilayered structures created by Laser-PTA additive manufacturing. *Mater Sci Eng A* 2022;830:142299.
- [89] Ling W, Wang X, Wang L, Wang X, Zhan X. Defect formation mechanism of laser additive manufacturing joint for large-thickness Ti6Al4V titanium alloy with Y2O3 nanoparticles. *Opt Laser Technol* 2023;157:108648.
- [90] Qin L, Wang K, Li X, Zhou S, Yang G. Review of the Formation Mechanisms and Control Methods of Geometrical Defects in Laser Deposition Manufacturing. *Chin J Mech Eng: Addit Manuf Front* 2022;1:100052.
- [91] Khajehmirza H, Astaraee AH, Monti S, Guagliano M, Bagherifard S. A hybrid framework to estimate the surface state and fatigue performance of laser powder bed fusion materials after shot peening. *Appl Surf Sci* 2021;567:150758.
- [92] Liu F, Xie H, He W. Multi-field coupling fatigue behavior of laser additively manufactured metallic materials: a review. *J Mater Res Technol* 2023;22:2819–43.
- [93] Sanaei N, Fatemi A. Defects in additive manufactured metals and their effect on fatigue performance: A state-of-the-art review. *Prog Mater Sci* 2021;117:100724.
- [94] Balbaa MA, Ghasemi A, Fereiduni E, Elbestawi MA, Jadhav SD, Kruth JP. Role of powder particle size on laser powder bed fusion processability of AlSi10mg alloy. *Addit Manuf* 2021;37:101630.
- [95] Mussatto A. Research progress in multi-material laser-powder bed fusion additive manufacturing: A review of the state-of-the-art techniques for depositing multiple powders with spatial selectivity in a single layer. *Results Eng* 2022;16:100769.
- [96] Boutaous M, Liu X, Signer DA, Xin S. Balling phenomenon in metallic laser based 3D printing process. *Int J Therm Sci* 2021;167:107011.

- [97] Wei HL, Mukherjee T, Zhang W, Zuback JS, Knapp GL, De A, DebRoy T. Mechanistic models for additive manufacturing of metallic components. *Prog Mater Sci* 2021;116:100703.
- [98] Vukkum VB, Gupta RK. Review on corrosion performance of laser powder-bed fusion printed 316L stainless steel: Effect of processing parameters, manufacturing defects, post-processing, feedstock, and microstructure. *Mater Des* 2022;221:110874.
- [99] Gunenthiram V, Peyre P, Schneider M, Dal M, Coste F, Koutiri I, Fabbro R. Experimental analysis of spatter generation and melt-pool behavior during the powder bed laser beam melting process. *J Mater Process Technol* 2018;251:376–86.
- [100] Nandakumar R, Venkatesan K. A process parameters review on selective laser melting-based additive manufacturing of single and multi-material: Microstructure, physical properties, tribological, and surface roughness. *Materials Today: Communications* 2023;35:105538.
- [101] Caballero A, Suder W, Chen X, Pardal G, Williams S. Effect of shielding conditions on bead profile and melting behaviour in laser powder bed fusion additive manufacturing. *Addit Manuf* 2020;34:101342.
- [102] Svetlizky D, Das M, Zheng B, Vyatskikh AL, Bose S, Bandyopadhyay A, Schoenung JM, Lavernia EJ, Eliaz N. Directed energy deposition (DED) additive manufacturing: Physical characteristics, defects, challenges and applications. *Mater Today* 2021;49:271–95.
- [103] Li Z, Sui S, Ma X, Tan H, Zhong C, Bi G, Clare AT, Gasserf A, Chen J. High deposition rate powder- and wire-based laser directed energy deposition of metallic materials: A review. *Int J Mach Tools Manuf* 2022;181:103942.
- [104] Manvatkar V, De A, DebRoy T. Heat transfer and material flow during laser assisted multi-layer additive manufacturing. *J Appl Phys* 2014;116:124905.
- [105] Zheng D, Li Z, Jiang Y, Li R, Wu Y, Tu Y, Cheng X, Fu P, Peng L, Tang H. Effect of multiple thermal cycles on the microstructure evolution of GA151K alloy fabricated by laser-directed energy deposition. *Addit Manuf* 2022;57:102957.
- [106] Zhang B, Ding H, Meng AC, Nemati S, Guo S, Meng WJ. Crack reduction in Inconel 939 with Si addition processed by laser powder bed fusion additive manufacturing. *Addit Manuf* 2023;72:103623.
- [107] Afkhami S, Lipiaiken K, Javaheri V, Amraei M, Salminen A, Bjork T. Effects of notch-load-defect interactions on the local stress-strain fields and strain hardening of additively manufactured 18Ni300 steel. *Mater Sci Eng A* 2023;876:145165.
- [108] Jia W, Chen S, Wang L, Shang F, Sun X, Yang D. Microstructure and properties of Ni-Co-Mn-Al magnetic shape memory alloy prepared by direct laser deposition and heat treatment. *Opt Laser Technol* 2021;141:107119.
- [109] Kempen K, Thijss L, Vrancken B, Buls S, Van HJ, Kruth JP. Producing crack-free, high density M2 Hss parts by selective laser melting: pre-heating the baseplate. *International Solid Freeform Fabrication Symposium*. University of Texas at Austin, 2013.
- [110] Yu J, Lin X, Ma L, Wang J, Fu X, Chen J, Huang W. Influence of laser deposition patterns on distortion, interior quality and mechanical properties by laser solid forming (LSF). *Mater Sci Eng A* 2011;528:1094–104.
- [111] Aliyu AAA, Poungsiri K, Shinjo J, Panwisawas C, Reed RC, Puncreobutr C, Tumkanon K, Kuimalee S, Lohwongwatana B. Additive manufacturing of tantalum scaffolds: Processing, microstructure and process-induced defects. *Int J Refrac Met Hard Mater* 2023;112:106132.
- [112] Siddiqui S, Araiza E. Microstructural defects governing torsional fatigue failure of additively manufactured as-built and heat-treated Inconel 718. *Eng Fail Anal* 2023;144:106975.
- [113] Gordon JV, Narra SP, Cunningham RW, Liu H, Chen H, Suter RM, Beuth JL, Rollett AD. Defect structure process maps for laser powder bed fusion additive manufacturing. *Addit Manuf* 2020;36:101552.
- [114] Yu T, Zhao J. Quantifying the mechanisms of keyhole pore evolutions and the role of metal-vapor condensation in laser powder bed fusion. *Addit Manuf* 2023;72:103642.
- [115] Gong H, Khalid R, Gu H, Thomas S, Brent S. Analysis of defect generation in Ti-6Al-4V parts made using powder bed fusion additive manufacturing processes. *Addit Manuf* 2014;1:4–87–98.
- [116] Bustillos J, Kim J, Moridi A. Exploiting lack of fusion defects for microstructural engineering in additive manufacturing. *Addit Manuf* 2021;48:102399.
- [117] Svetlizky D, Zheng B, Buta T, Zhou Y, Golan O, Breiman U, Rami HA, Julie MS, Enrique JL, Noam E. Directed energy deposition of Al 5xxx alloy using Laser Engineered Net Shaping (LENS®). *Mater Des* 2020;192:108763.
- [118] Abadi SMANR MiY, Kisielewicz A, Sikström F, Choquet I. Influence of laser-wire interaction on heat and metal transfer in directed energy deposition. *Int J Heat Mass Transf* 2023;205:123894.
- [119] Chu LAL, Sebastian M, Michael T, Robert CA, Philip JW, Peter DL. The effect of powder oxidation on defect formation in laser additive manufacturing. *Acta Mater* 2019;166:294–305.
- [120] Zhang L, Zhai W, Zhou W, Chen X, Chen L, Han B, Cao L, Bi G. Improvement of mechanical properties through inhibition of oxidation by adding TiC particles in laser aided additive manufacturing of stainless steel 316L. *Mater Sci Eng A* 2022;853:143767.
- [121] Guo L, Zhang L, Andersson J, Ojo O. Additive manufacturing of 18% nickel maraging steels: Defect, structure and mechanical properties: A review. *J Mater Sci Technol* 2022;120:227–52.
- [122] Cao Y, Wei HL, Yang T, Liu TT, Liao WH. Printability assessment with porosity and solidification cracking susceptibilities for a high strength aluminum alloy during laser powder bed fusion. *Addit Manuf* 2021;46:102103.
- [123] Wang MS, Liu EW, Du YL, Liu TT, Liao WH. Cracking mechanism and a novel strategy to eliminate cracks in TiAl alloy additively manufactured by selective laser melting. *Scr Mater* 2021;204:114151.
- [124] Li R, Niu P, Yuan T, Li Z. Displacive transformation as pathway to prevent micro-cracks induced by thermal stress in additively manufactured strong and ductile high-entropy alloys. *Trans Nonferrous Met Soc China* 2021;31:1059–73.
- [125] Xie D, Lv F, Yang Y, Shen L, Tian Z, Shuai C, Cheng B, Zhao J. A Review on Distortion and Residual Stress in Additive Manufacturing. *Chin J Mech Eng: Addit Manuf Front* 2022;1:100039.
- [126] Desai RK. Process Control Strategies in Additive Manufacturing. Rutgers The State University of New Jersey. School of Graduate Studies.; 2019.
- [127] Gonon S, Yuval C. A framework for smart control using machine-learning modeling for processes with closed-loop control in Industry 4.0. *Eng Appl Artif Intell* 2021;102:104236.
- [128] Rawat D, Gupta MK, Sharma A. Intelligent control of robotic manipulators: a comprehensive review. *Spat Inf Res* 2023;31:345–57.
- [129] Saif AW. A Frame Work for the Integration of Statistical Process Control and Engineering Process Control. 2019 Industrial & Systems Engineering Conference (ISEC). IEEE.; 2019. p. 1–4.
- [130] Adauto B, Moacir GF, Alejandro GF. Smart production planning and control in the Industry 4.0 context: A systematic literature review. *Comput Ind Eng* 2020;149:106774.
- [131] Kim DH, Kim TJ, Wang X, Kim M, Quan YJ, Oh JW, Min SH, Kim H, Bhandari B, Yang I, Ahn SH. Smart machining process using machine learning: A review and perspective on machining industry. *Int J Precis Eng Manuf-Green Technol* 2018;5:555–68.
- [132] Chao L, Léopold LR, Ze J, Pierre K, Franck L, Samuel B. Machine Learning-enabled feedback loops for metal powder bed fusion additive manufacturing. *Procedia Comput Sci* 2020;176:2586–95.
- [133] Parsazadeh M, Sharma S, Dahotre N. Towards the next generation of machine learning models in additive manufacturing: A review of process dependent material evolution. *Prog Mater Sci* 2023;135:101102.
- [134] Goh GD, Sing SL, Yeong WY. A review on machine learning in 3D printing: applications, potential, and challenges. *Artificial Intell Rev* 2021;54:63–94.
- [135] Guo S, Agarwal M, Cooper C, Tian Q, Gao RX, Guo W, Guo YB. Machine learning for metal additive manufacturing: Towards a physics-informed data-driven paradigm. *J Manuf Syst* 2022;62:145–63.
- [136] Johnson NS, Vulimiri PS, To AC, Zhang X, Brice CA, Kappes BB, Stebner AP. Invited review: Machine learning for materials developments in metals additive manufacturing. *Addit Manuf* 2020;36:101641.
- [137] Aoyagi K, Wang H, Sudo H, Chiba A. Simple method to construct process maps for additive manufacturing using a support vector machine. *Addit Manuf* 2019;27:353–62.
- [138] Wang R, Standfield B, Dou C, Law AC, Kong ZJ. Real-time process monitoring and closed-loop control on laser power via a customized laser powder bed fusion platform. *Addit Manuf* 2023;66:103449.
- [139] Garanger K, Khamvilai T, Feron E. Validating feedback control to meet stiffness requirements in additive manufacturing. *IEEE Trans Control Syst Technol* 2020;28:2053–60.
- [140] Rezaeifar H, Elbestawi MA. On-line melt pool temperature control in L-PBF additive manufacturing. *Int J Adv Manuf Technol* 2021;112:2789–804.
- [141] Tristan GF, Stephen GL, Nestor TR, Allen MAB, Nathan JS, James MF. Tracking and controlling the morphology evolution of 3D powder-bed fusion *in situ* using inline coherent imaging. *Addit Manuf* 2020;32:100978.
- [142] Rienzsche A, Bevans BD, Smoqi Z, Yavari R, Krishnan A, Gilligan J, Piercy N, Cole K, Rao P. Feedforward control of thermal history in laser powder bed fusion: Toward physics-based optimization of processing parameters. *Mater Des* 2022;224:111351.
- [143] Drzuzalski CL, Ashby A, Guss G, King WE, Roehling TT, Matthews MJ. Process optimization of complex geometries using feed forward control for laser powder bed fusion additive manufacturing. *Addit Manuf* 2020;34:101169.
- [144] Wang D, Chen X. Closed-loop simulation integrating finite element modeling with feedback controls in powder bed fusion additive manufacturing. *International Symposium on Flexible Automation*. American Society of Mechanical Engineers.; 2020. p. 83617.
- [145] Wang Q, Michaleris PP, Abdalla RN, Jeffrey EI, Ren Y, Christopher BS. Model-based feedforward control of laser powder bed fusion additive manufacturing. *Addit Manuf* 2020;31:100985.
- [146] Hussain SZ, Kausar Z, Koreshi ZU, Sheikh SR, Rehman HZU, Yaqoob H, Muhammad FS, Ahmad A, Sher F. Feedback Control of Melt Pool Area in Selective Laser Melting Additive Manufacturing Process. *Processes* 2021;9:1547.
- [147] Volker R, Stephan A, Gert G, Arne N, Claus E. Development of an adaptive, self-learning control concept for an additive manufacturing process. *CIRP J Manuf Sci Technol* 2017;19:57–61.
- [148] Yang Z, Lu Y, Yeung H, Krishnamurti S. Investigation of deep learning for real-time melt pool classification in additive manufacturing. 2019 iee 15th International Conference on Automation Science and Engineering (case). IEEE.; 2019. p. 640–7.
- [149] Francis O, Amir BF. Thermal control of laser powder bed fusion using deep reinforcement learning. *Addit Manuf* 2021;46:102033.
- [150] Zhong Q, Tian X, Huang X, Huo C, Li D. Using feedback control of thermal history to improve quality consistency of parts fabricated via large-scale powder bed fusion. *Addit Manuf* 2021;42:101986.
- [151] Su Y, Wang Z, Xu X, Luo K, Lu J. Effect of closed-loop controlled melt pool width on microstructure and tensile property for Fe-Ni-Cr alloy in directed energy deposition. *J Manuf Process* 2022;82:708–21.

- [152] Baraldo S, Vandone A, Valente A, Carpanzano E. Vision-based control for track geometry optimization of complex AM motion profiles by on-line laser power modulation. *Procedia CIRP* 2020;95:78–82.
- [153] Xu P, Yao X, Chen L, Zhao C, Liu K, Moon SK, Bi G. In-process adaptive dimension correction strategy for laser aided additive manufacturing using laser line scanning. *J Mater Process Tech* 2022;303:117544.
- [154] Tang L, Landers RG. Melt pool temperature control for laser metal deposition processes-part II: layer-to-layer temperature control. *J Manuf Sci Eng* 2010;132:011011.
- [155] Liao S, Webster S, Huang D, Council R, Ehmann K, Cao J. Simulation-guided variable laser power design for melt pool depth control in directed energy deposition. *Addit Manuf* 2022;56:102912.
- [156] Ding Y, James W, Radovan K. Development of sensing and control system for robotized laser-based direct metal addition system. *Addit Manuf* 2016;10:24–35.
- [157] Shi T, Lu B, Shen T, Zhang R, Shi S, Fu G. Closed-loop control of variable width deposition in laser metal deposition. *Int J Adv Manuf Technol* 2018;97:4167–78.
- [158] Li P, Ji S, Zeng X, Hu Q, Xiong W. Direct laser fabrication of thin-walled metal parts under open-loop control. *Int J Mach Tools Manuf* 2007;47:996–1002.
- [159] Hofman JT, Pathiraj B, Dijk JV, Lange DFD, Meijer J. A camera-based feedback control strategy for the laser cladding process. *J Mater Process Technol* 2012;212:2455–62.
- [160] Zeinali M, Amir K. Height control in laser cladding using adaptive sliding mode technique: theory and experiment. *J Manuf Sci Eng* 2010;132:041016.
- [161] Meysam A, Radovan K. Closed loop control of melt pool width in robotized laser powder-directed energy deposition process. *Int J Adv Manuf Technol* 2019;104:2887–98.
- [162] Farshidianfar MH, Khajepour A, Zeinali M, Gelrich A. System identification and height control of laser cladding using adaptive neuro-fuzzy inference systems. *Int Congr Appl Lasers Electro-Opt* 2013;1:615–23.
- [163] Masanori M, Takeshi T, Hirotsugu K. Adaptive shape control of laser-deposited metal structures by adjusting weld pool size. *J Laser Appl* 2014;26:032003.
- [164] Farshidianfar MH, Khajepour A, Gerlich A. Real-time control of microstructure in laser additive manufacturing. *Int J Adv Manuf Technol* 2016;82:1173–86.
- [165] Nassar AR, Keist JS, Reutzel EW, Spurgeon TJ. Intra-layer closed-loop control of build plan during directed energy additive manufacturing of Ti-6Al-4V. *Addit Manuf* 2015;6:39–52.
- [166] Farshidianfar MH, Khodabakhshi F, Khajepour A, Gerlich AP. Closed-loop deposition of martensitic stainless-steel during laser additive manufacturing to control microstructure and mechanical properties. *Opt Lasers Eng* 2021;145:106680.
- [167] Farshidianfar MH, Khodabakhshi F, Khajepour A, Gerlich AP. Closed-loop control of microstructure and mechanical properties in additive manufacturing by directed energy deposition. *Mater Sci Eng: A* 2021;803:140483.
- [168] Su Y, Wang C, Xu X, Luo K, Lu J. Pore defects and corrosion behavior of AISI 316L stainless steel fabricated by laser directed energy deposition under closed-loop control. *Surf Coat Technol* 2023;463:129527.
- [169] Tyralla D, Köhler H, Seefeld T, Thomy C, Narita R. A multi-parameter control of track geometry and melt pool size for laser metal deposition. *Procedia CIRP* 2020;94:430–5.
- [170] Guo Z, Bi G, Wei J. Design of a novel control strategy for laser-aided additive manufacturing processes. *IECON 2016-42nd Annual Conference of the IEEE Industrial Electronics Society*. IEEE.; 2016. p. 6091–6.
- [171] Takushima S, Shinohara N, Morita D, Kawano H, Mizutani Y, Takaya Y. In-Process Height displacement measurement using crossed line beams for process control of laser wire deposition. *Int J Autom Technol* 2021;15:715–27.
- [172] Gibson BT, Richardson BS, Sundermann TW, Love LJ. Beyond the toolpath: Site-specific melt pool size control enables printing of extra-toolpath geometry in Laser Wire-Based directed energy deposition. *Appl Sci* 2019;9:4355.
- [173] Gibson BT, Bandari YK, Richardson BS, Henry WC, Vetland EJ, Sundermann TW, Love LJ. Melt pool size control through multiple closed-loop modalities in laser-wire directed energy deposition of Ti-6Al-4V. *Addit Manuf* 2020;32:100993.
- [174] Tyralla D, Seefeld T. Temperature field based closed-loop control of laser hot wire cladding for low dilution. *Procedia CIRP* 2020;94:451–5.
- [175] Almir H, Christiansson AK, Ottosson M, Lennartson B. Increased stability in laser metal wire deposition through feedback from optical measurements. *Opt Lasers Eng* 2010;48:478–85.
- [176] Garmendia I, Pujana J, Lamikiz A, Flores J, Madarieta M. Development of an intra-layer adaptive toolpath generation control procedure in the laser metal wire deposition process. *Materials* 2019;12:352.
- [177] Huang W, Chen S, Xiao J, Jiang X, Jia Y. Laser wire-feed metal additive manufacturing of the Al alloy. *Opt Laser Technol* 2021;134:106627.
- [178] Häggqvist P, Heralić A, Christiansson AK, Lennartson B. Resistance based iterative learning control of additive manufacturing with wire. *Mechatronics* 2015;31:116–23.
- [179] Teichmann EW, Kelbassa J, Gasser A, Tarner S, Schleifenbaum JH. Effect of wire feeder force control on laser metal deposition process using coaxial laser head. *J Laser Appl* 2021;33:012041.
- [180] Heralić A, Christiansson AK, Lennartson B. Height control of laser metal-wire deposition based on iterative learning control and 3D scanning. *Opt Lasers Eng* 2012;50:1230–41.